INVESTIGATION OF FRP STABILIZATION OF PLASTIC BUCKLING BEHAVIOR OF SLENDER STEEL SECTIONS

by

Andrew Jeffrey Peck

Bachelor of Science in Civil Engineering, University of Michigan, Ann Arbor, 2006

Submitted to the Graduate Faculty of

The School of Engineering in partial fulfillment

of the requirements for the degree of

Master of Science

University of Pittsburgh

2007

UNIVERSITY OF PITTSBURGH

SCHOOL OF ENGINEERING

This thesis was presented

by

Andrew Jeffrey Peck

It was defended on

December 3rd, 2007

and approved by

Dr. Amir Koubaa, Academic Coordinator and Lecturer,
Department of Civil and Environmental Engineering

Dr. Piervincenzo Rizzo, Assistant Professor,
Department of Civil and Environmental Engineering

Dr. Kent A. Harries, William Kepler Whitford Faculty Fellow and Assistant Professor,
Department of Civil and Environmental Engineering
Thesis Advisor

INVESTIGATION OF FRP STABILIZATION OF PLASTIC BUCKLING BEHAVIOR
OF SLENDER STEEL SECTIONS

Andrew Peck, M.S.

University of Pittsburgh, 2007

An innovative use of fiber reinforced polymer (FRP) composite materials, to control the manifestation of local buckling in a flanged steel section, is proposed. In this method, the high stiffness and linear behavior of FRP materials are utilized to provide "bracing" against web or flange local buckling in a manner that strategically leverages the unique mechanical properties of each material in an efficient application domain. The experimental research reported is aimed at demonstrating the feasibility of using small quantities of FRP to provide cross-sectional stability through the bonding of FRP strips to flange elements of the cross-section, thereby increasing the critical load of the member; constraining plastic flow in the cross-sectional flange elements; and facilitating the manifestation of a well-formed and stable hysteretic response of the member under cyclic loading. The member becomes, in effect, an *FRP stabilized steel section*.

An experimental program investigating the inelastic buckling behavior of FRP stabilized members is reported. In all cases, WT 6x7 steel sections were used. Unretrofit control specimens and four retrofit scenarios were investigated using either high strength (HS) carbon FRP (CFRP) strips or ultra-high modulus (UHM) glass FRP (GFRP) strips.

For each material two cases were considered: a single 2 in. (50.8 mm) wide strip applied to the WT stem; and two 1 in. (25.4 mm) wide strips placed on top of each other at the same location. The FRP strips were applied to each side of the WT stem. The two FRP configurations used result in the same area of FRP materials having the same centroid applied to the steel section.

Fifteen 14 in. (356 mm) long WT sections were tested in concentric compression to failure. Three specimens of each detail were tested. The specimen length was selected to ensure local buckling of the WT stem with no lateral torsional buckling of the section. Each specimen was dominated by web (stem) local buckling (WLB) behavior. No evidence of flange local buckling or lateral torsional buckling was observed. The presence of the FRP increased the axial load carrying capacity of the WT section between 4% and 14%. The bifurcation loads were increased as much as 17%. In these tests, the CFRP specimens exhibited a more pronounced improvement in behavior. Similarly, the specimens having two 1 in. wide FRP strips performed better that those with one 2 in. strip. Debonding of the FRP strips was a post-peak phenomenon in all tests. Generally debonding occurred at an applied load of about 75% of the peak load on the descending branch of the load curve.

TABLE OF CONTENTS

LIST OF TABLES

LIST OF FIGURES

NOMENCLATURE

Abbreviations

AISC   American Institute of Steel Construction

CFRP   carbon fiber-reinforced polymer

CISC   Canadian Institute of Steel Construction

DWT   draw wire transducer

FLB   flange local buckling

FRP   fiber-reinforced polymer

GFRP   glass fiber-reinforced polymer

hmCFRP   high modulus carbon fiber-reinforced polymer

hsCFRP   high strength carbon fiber-reinforced polymer

LTB   lateral torsional buckling

LRFD   load and resistance factor design

uhmCFRP   ultra high modulus carbon fiber-reinforced polymer

WLB   web local buckling

Notation

A_g gross area

b   flange width

C_r first buckling load of bracing members

d   depth of the cross section

δ   axial deformation

Δ   lateral displacement at midlength

ε   strain

e_x loading eccentricity about the strong axis

e_y loading eccentricity about the weak axis

E   Young's modulus

F_{cr} local buckling critical load

F_{crft} flexural torsional buckling capacity

F_{cry} critical buckling stress

F_e elastic critical buckling stress (Euler buckling stress)

F_y yield stress

G_a shear modulus

KL   effective buckling length

λ   KL/r; slenderness ratio

$λ_p$ limiting width-thickness ratio

$λ_c$ column slenderness parameter

P   axial load

P_{cr} critical buckling load

Q_s Euler buckling reduction factor

r_y radius of gyration about the weak axis

t_a thickness of adhesive layer

t_f flange thickness

t_w web thickness

ACKNOWLEDGEMENTS

Firstly, I would like to thank my thesis advisor and committee chair, Dr. Kent A. Harries for his guidance and assistance throughout my graduate education and the entire thesis process. I am indebted to him for the vast amount of time and effort he has provided towards me throughout my graduate career at the University of Pittsburgh.

In addition, I would like to thank my committee members Dr. Piervincenzo Rizzo and Dr. Amir Koubaa for their support and constructive criticism throughout the thesis process.

I would also like to acknowledge my fellow graduate student, Karthik Ramanathan, for his assistance during the research and execution of the experimental portion of my thesis. Also, I would like to thank the undergraduate students, Lou Gualtieri and Parker Webb, for their assistance in performing the experimental procedure of the thesis.

I would like to thank my parents for their love and support not only during my thesis and educational career, but through all aspects of my life.

Finally, I would like to thank the following companies for supplying the materials necessary to make this research possible: Fyfe Company LLC, San Diego, CA, and Fox Industries.

1.0   INTRODUCTION

An innovative use of fiber reinforced polymer (FRP) composite materials, to control the manifestation of local buckling in a flanged steel section, is proposed. In this method, the high stiffness and linear behavior of FRP materials are utilized to provide "bracing" against web or flange local buckling in a manner that strategically leverages the unique mechanical properties of each material in an efficient application domain. The experimental research reported is aimed at demonstrating the feasibility of using small quantities of FRP to provide cross-sectional stability through the bonding of FRP strips to flange elements of the cross-section, thereby increasing the critical load of the member; constraining plastic flow in the cross-sectional flange elements; and facilitating the manifestation of a well-formed and stable hysteretic response of the member under cyclic loading. The member becomes, in effect, an *FRP stabilized steel* section.

Extensive advances in the application of fiber reinforced polymer (FRP) composite materials for repair and strengthening of structures and their components have been made. The merits of FRP retrofit of reinforced concrete members have been well researched and documented. Relatively limited work however has been conducted investigating the use of FRP to retrofit steel members (Zhao and Zhang, 2006). Carbon FRP (CFRP) materials have been used to strengthen steel members (e.g.: Cadei et al., 2004; Miller et al., 2004), enhance fatigue or fracture performance (e.g.: Jones and Civjan, 2003) and provide local stability for steel compression members (e.g.: Ekiz and

1

El-Tawil, 2006; Shaat and Fam, 2004). The present work proposes the concept of an FRP stabilized steel section. It is proposed that through the strategic application of FRP to a steel compression member a degree of buckling restraint may be affected.

The linear behavior, high strength, and stiffness of FRP materials can be applied to a steel section to increase member stability. More specifically, small amounts of FRP can be utilized to increase resistance to flange (FLB) and/or web (WLB) local buckling. The purpose of such an application is not necessarily to increase load-carrying capacity but to restrict plastic flow of the plate member. A schematic representation of the concept of FRP stabilization and the test specimens used and their behavior is shown in Figure 1.1.

1.1   SUMMARY OF RESEARCH PROGRAM

An experimental program investigating the inelastic buckling behavior of FRP stabilized members is reported. In all cases, WT 6x7 steel sections were used. Unretrofit control specimens and four retrofit scenarios were investigated using either high strength (HS) CFRP strips or ultra-high modulus (UHM) GFRP strips. For each material two cases were considered: a single 2 in. (50.8 mm) wide strip applied to the WT stem; and two 1 in. (25.4 mm) wide strips placed on top of each other at the same location. The FRP strips were applied to each side of the WT stem. The two FRP configurations used result in the same area of FRP materials having the same centroid applied to the steel section.

Fifteen 14 in. (356 mm) long WT sections were tested in concentric compression to failure. Three specimens of each detail were tested. The specimen length was selected to ensure local buckling of the WT stem with no lateral torsional buckling (LTB) of the section. Each specimen was dominated by web (stem) local buckling (WLB). No evidence of FLB or LTB was observed. The presence of the FRP increased the axial load carrying capacity of the WT section between 4% and 14%. The bifurcation loads were increased as much as 17%. In these tests, the CFRP specimens exhibited a more pronounced improvement in behavior. Similarly, the specimens having two 1 in. wide FRP strips performed better that those with one 2 in. strip. Debonding of the FRP strips was a post-peak phenomenon in all tests. Generally debonding occurred at an applied load of about 75% of the peak load on the descending branch of the load curve.

1.2   OBJECTIVES OF RETROFIT

When retrofitting steel sections with FRP, the objectives may be a combination of a) increasing the maximum compressive capacity of the member; and b) increasing the radius of gyration to improve the buckling behavior. Additionally, the more slender a member, the more the member behavior deteriorates under cyclic loading (Bruneau et al., 1998). Decreasing the slenderness of a member ultimately increases the cyclic loading lifespan as well as its loading capacity.

The slenderness ratio of a compression member is a function of member length and radius of gyration. In this study, the stem of the WT section tested is locally very

3

slender and presents a specific region at which to concentrate the FRP retrofit application. Considering only the WT stem, the increase in weak-axis radius gyration (r_y) due the application of the FRP ranged from 12% to 35%. This suggests the prospect of increasing stability on a local level. However, a negligible increase in r_y is determined when the entire WT cross section is considered; thus there is a negligible effect on the global brace behavior. The FRP-retrofitted members tested mirror this predicted behavior where the increases in radius of gyration are proportional to, although approximately three times, the observed increases in axial load carrying capacity and bifurcation load in the inelastic stub column tests.

1.3   SCOPE OF THESIS

The objective of the work reported in this thesis is to assess the effectiveness of FRP composite materials for mitigating inelastic buckling behavior of steel sections. The work reported here should be considered a pilot study to assess the feasibility of such an approach. Ultimately, if FRP composite materials prove to provide support for steel members under inelastic behavior, it may be feasible to improve the cyclic load capacity of members susceptible to WLB and FLB. Since the behavior of FRP stabilized steel members is still in its infancy in terms of research, it is the goal of this report to provide a more thorough understanding of the applications of FRP in this situation. This thesis focuses on the effects of FRP on axially loaded steel members under inelastic buckling in terms of; peak load capacity, web bifurcation load, radius of gyration, the effects on the

stem in axial compression, and the debonding of the FRP composite material from the steel substrate are discussed.

The organization of the thesis is as follows. Chapter 2 presents a thorough review of available literature focusing on the use of FRP to retrofit steel members, specifically for stability. Section 2.7 demonstrates the potential "design space" for FRP stabilization and Section 2.8.1 provides a brief summary of a companion study addressing elastic buckling behavior. Chapter 3 presents details of the experimental program conducted. Chapter 4 presents detailed results of the experimental program. A discussion of the results is presented in Chapter 5. Chapter 6 provides a summary of the program, conclusions and recommendations.
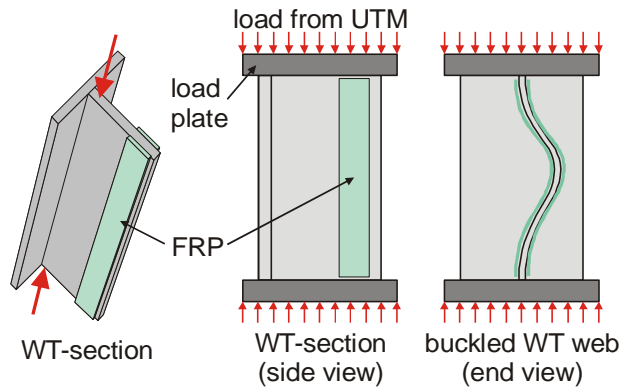
Figure 1.1 Schematic representation of test specimens and behavior.

2.0   LITERATURE REVIEW

The study reported in this thesis was conducted to investigate the use of fiber reinforced polymer (FRP) composite materials for the stabilization of local plastic buckling of slender steel sections. The use of FRP composite materials in a flanged steel section was ultimately studied to investigate the ability to control aspects of the manifestation of local buckling. FRP is a material which exhibits linear elastic behavior to failure. This behavior, it is proposed, may be used to provide the necessary bracing force to limit web or flange local buckling in a steel member. By applying small quantities of FRP composite materials to the web of WT 6x7 sections, it was hypothesized that the stability of the very slender web would improve. Such an improvement may result in increased critical load capacity and mitigation of the capacity loss and "kinking" effects associated with compression buckling under cyclic loading. By constraining these plastic flow effects within a slender element, a well-formed and stable hysteretic response under cyclic loading of the slender steel member may be achieved. This concept has been introduced and is referred to as FRP stabilized steel sections (Accord et al., 2006; Abraham and Harries, 2007). Previous experimental work has focused on the elastic buckling behavior of FRP stabilized steel sections (Abraham, 2006). The focus of this work is the affects of FRP stabilization on a steel member prone to inelastic buckling. This application is believed to be unique but builds on previous applications of FRP in civil infrastructure as discussed in the following sections.

2.1   FRP MATERIALS

Fiber reinforced polymer (FRP) materials combine high-modulus, high strength fibers with a relatively low-modulus polymeric matrix to produce a material having high unit strength and unit stiffness. The polymeric matrix serves to protect the fibers and transfer load between fibers, ensuring a uniform behavior. The strength of FRP is dependent upon both the fiber type and orientation. FRP composite materials with high fiber volume ratios are typically found in the civil engineering industry. One of the great advantages FRP composite materials brings to the civil engineering industry, is their ability to safely carry large loads and the ease with which they may be employed to retrofit existing structures (Harries and El-Tawil, 2006).

Two of the most common types of FRP composite materials are those made with carbon (CFRP) and glass (GFRP) fibers. CFRP can be found in three basic types; high strength (hsCFRP), high modulus (hmCFRP), and ultra-high modulus (uhmCFRP). Generally speaking, when the stiffness of CFRP is increased, there is a corresponding reduction in strength and rupture strain of the FRP material. GFRP, compared to CFRP, has a much lower modulus but is often more cost effective on the basis of unit stiffness. When determining the proper type of FRP for a retrofit, it is best to choose a FRP composite material that has a modulus which is compatible to the substrate to which the FRP is being applied. CFRP has largely been chosen in retrofitting steel members for this reason (Harries and El-Tawil, 2006).

The mechanics of the FRP itself are extremely refined in themselves. The individual fibers, yarns or tows (for a glossary of FRP terms used in civil infrastructure, consult ACI 440R-07) are protected and bound by the polymeric matrix, distributing the force between the fibers through interfacial shear and providing a degree of stability to the fibers. Not only does the matrix act as a force transferring system, but it also aids in protection of the fiber material from the surrounding environment. The most common FRP systems use epoxy-based resin systems. Similarly, when preformed FRP materials are used, epoxy-based adhesive systems are preferred for their strength, durability and ease of use. When utilizing FRP composite materials to retrofit a steel substrate, one must fully understand the resulting steel-adhesive-FRP system in order to comprehend the behavior of the new structural system. Table 2.1 provides typical properties of the steel-adhesive-FRP systems.

2.2   STRENGTHENING OF STEEL USING FRP MATERIALS

Moy (2004a) proposed design guidelines for the strengthening of metallic structures using FRP materials. These guidelines are formalized in CIRIA's (UK) Report C595 (Cadei et al. 2004). According to Moy, when strengthening metallic materials with FRP, several limit states must be considered. The foremost limit state would be the ultimate limit state, which would be the partial or total collapse of a structure due to the failure of: a) the FRP in tension or compression; b) the metallic substrate; c) the adhesive joint; or d) the local or global buckling of the member. One must also consider the serviceability limit state,

addressing member deflection, deformation, or vibration. When utilizing FRP materials to strengthen metallic structures, it is also imperative to verify that the retrofit will be durable, introducing a third limiting state focused on time or aging related effects, such as: fatigue, creep, corrosion, and weathering. Finally, one must consider abnormal or extreme events such as fire, mechanical impact (collision) and/or seismic resistance, when retrofitting with FRP composite materials. To address many of these limit states the application process of the FRP is often critical. When applying FRP to metallic substrates it is essential that the substrate surface is clean and clear of blemishes, such as corrosion, to ensure a sound bond between the FRP and the metallic substrate. It is further noted by Moy that GFRP composite material is seldom used when strengthening metallic structures due to its low modulus of elasticity.

As with any retrofitting material, the ultimate strength provided is only as good as the idyllic creation of the FRP composite material itself. This, as in every other aspect of design engineering, is why safety factors are applied to design codes. A primary concern when retrofitting any metallic structure with FRP is the long term degradation that may accompany the retrofit based on the surrounding environment. In particular corrosion or continued corrosion of the steel substrate may have significant effects on the bond behavior of the FRP. Degradation of strength, stiffness or bond properties may be caused by several factors (and their synergies), including; exposure to moisture, ultra-violet light, chemical exposure, fatigue, and creep. As proposed by Moy (2004a), Table 2.2 displays a list of partial safety factors proposed for different environmental exposures and different FRP materials. Such factors would be applied in addition to code-prescribed material resistance or load factors. It

9

can be seen in Table 2.2, that CFRP is generally the most inert of the conventional forms of FRP material.

When strengthening a metallic structure with a FRP composite system, it is also essential to optimize the epoxy bond strength between the substrate and the FRP. Poor bond will hinder the performance of the FRP composite system, ultimately decreasing the effectiveness of the retrofit. Regular inspections of retrofitted FRP composite metallic structures are necessary to ensure the safety and durability of the system (Moy, 2004a).

The strengthening of steel members with FRP composite materials has been the subject of limited research over the past few years. Although the area of strengthening concrete with FRP composite materials has thoroughly advanced within the civil engineering industry, the use of such retrofits with steel is still in its relative infancy. With the advancement of composite materials, they become much more practical as lightweight and easily installable retrofit materials. Several studies on the strengthening effects of FRP on steel members have been conducted. Patnaik and Bauer (2004) studied the effects of CFRP laminates on the strengthening of steel beams in both flexure and shear. The beams tested under flexural loading were strengthened with CFRP on the tension flange and exhibited a 30% increase in load carrying capacity. The beams tested under shear were retrofitted with CFRP on the beam webs and exhibited a 62% increase in apparent shear capacity. They concluded that the composite retrofits strengthened the beam in both flexure and shear, and that composite FRP materials applied to steel warrant further investigation.

Sayed-Ahmed (2004) conducted an analytical study focused on the effects of local buckling on thin-webbed steel I-sections with CFRP applied to the areas of local buckling under compression. The main goal of this technique is to affect a delayed response in the

10

local buckling of the web of the beam. Based on an analytical study where CFRP was applied at the midheight of the web and assumed to result in a brace point at this location, Sayed-Ahmed concluded that the application of CFRP strips to these steel members not only increased the critical load of the member from 20-60%, but it also increased the ultimate strength by 2-9%. While the study was flawed, it nonetheless introduced the potential of FRP-stabilized steel members.

Miller et al. (2001), focused on the use of CFRP plates in strengthening a steel bridge girder on Interstate-95 in Newark, Delaware. The feasibility of such a retrofit was concluded, and the application in a real world scenario was carried out. It was determined that these retrofits provide great promise for retrofitting structures for increased strength. The CFRP plates theoretically increased the capacity corrosion damaged bridge girders from 10-37% (since this is an active Interstate, no tests to failure can be conducted). The CFRP resulted in an apparent increase of 11.6% in the structure's flexural stiffness. As with any real world scenario testing, further information can be retrieved from such applications to determine the long-term effectiveness of such retrofits. For instance, it was found that the inclusion of GFRP plates at the steel interface aided in the prevention of galvanic corrosion.

Shaat and Fam (2004) illustrated the use of FRP sheets for the strengthening of short HSS steel columns. The use of both CFRP and GFRP perimeter wraps were examined in axial compression tests of short HSS steel columns. By varying the fiber orientation and FRP layering it was determined that when two layers of CFRP wraps were both fixed in the transverse direction an axial strength capacity increase of 18% was recorded. In contrast, when one layer of the CFRP was oriented longitudinally, and the next layer is applied transversely, the axial stiffness is increased significantly by 28%. This demonstrates the

importance of fiber orientation in steel strengthening capacity. Not only did this test show the capacity of FRP retrofits to aid in the strengthening of steel, it also displayed the importance of bonding between the FRP and steel substrate to be a limiting factor in the capacity of the retrofit. This will be discussed further in following sections.

2.3   FATIGUE BEHAVIOR OF STEEL WITH FRP

The fatigue life of a steel structure is critical to the expected usable or remaining life of any structure. Jones and Civjan (2003) focused their studies on the application of fiber reinforced polymer overlays to extend the fatigue life of steel. It was noted through fatigue experiments that the reduced fatigue-induced stress in the steel, and thus improved behavior, attributed to the application of FRP materials is largely governed by the adhesive connection between the steel substrate and the FRP. Generally speaking, there was some demonstrated effectiveness in increasing of fatigue life, but the behavior of the steel element was entirely dominated by the adhesive behavior of the epoxy material.

Ekiz (2007) demonstrated improved steel brace fatigue behavior under either seismic or wind loading conditions using carbon fiber reinforced polymer (CFRP) wrapping. The improvement in a structure's ability to maintain greater stability under cyclic loading scenarios only furthers the potential benefits of the applications of FRP to steel structures. This application will be explored in the present work.

2.4   STRUCTURAL REHABILITATION USING FRP

Rehabilitation, that is: restoring capacity to, rather than specifically strengthening, a member or structure is presently of great interest in the civil infrastructure community due to the significant number of deteriorated structures. Through the use of fiber reinforced polymers, structural rehabilitation may be less time consuming and more easily accomplished over a broad spectrum of structures. Gillespie et al. (1996), using adhesively bonded FRP systems, demonstrated the rehabilitation of steel girders having significant corrosion. The use of composite materials showed great promise for increasing the structural life and stability of corrosion and fatigue damaged members. Even with corroded girders, it was determined that composite materials were able to provide significant rehabilitation effect to structural elements. Not only was the stiffness of the degraded members improved with the application of FRP composite materials, the desired loads were reached without adhesive failure between the steel substrate and the composite materials. Through further testing it was determined that fiber reinforcement additionally provided a means to reduce fatigue crack growth, ultimately increasing the life of the steel member, in turn leading to a longer life span of the structure. In this application it is noted that the ultimate strength of the structure was not completely returned to its "as built" value, however the rehabilitation restored sufficient capacity to safely resist present-day load demands.

Hollaway and Cadei (2002) explored the technique of upgrading metallic structures with FRP materials. Through their studies, it was concluded that with the application of FRP materials to existing metallic structural systems, the working life of a structure could be extended 1.5 times its original lifespan. In addition to this, the cost saving introduce by using

FRP were in the range of 17.5% over alternative steel rehabilitation methods. As previously mentioned, the adhesive bond of the FRP to the steel is extremely critical in this rehabilitation method. It is critical that both the FRP and steel substrates surfaces are properly prepared in order to maximize the epoxy bond. Not only did this report focus on the rehabilitation properties of FRP, but it also noted the use of GFRP in offshore platforms as a form of fire protection for the structural member. Thus GFRP has been used in prolonging the life of a structural element in extreme environments. These findings in the rehabilitation of both experimentally and field tested steel members through the use of FRP, demonstrate the practicality and promise of FRP in the field of structural rehabilitation.

2.5   BOND INTERFACE BETWEEN FRP AND STEEL SUBSTRATE

As discussed in previous sections, the interface bond between the fiber reinforced polymer (FRP) composite material and the steel substrate is one of, if not the most important factor determining in the effectiveness of FRP on the behavior of steel. The bond of the FRP to the steel substrate dictates the extent to which the FRP may aid the structural steel element in improving its capacity, ductility, and/or delaying effects of both local and lateral torsional buckling. Sebastian and Luke (2007) explored the interface failure mechanics of FRP reinforced steel beam members. These tests focused on the interface between steel beams and adhesively bonded elastic reinforcing strips to determine the stresses developed in the interface between the composite and the steel. Several variations of the composite material were tested on the steel substrate. First, the affects of multiple layers of the elastic FRP strips

were studied. The effects of tapering the composite material were analyzed in the determination of the plane stress interface between the steel and the composite material. To minimize bond stresses, the FRP should change in cross-sectional area with the moment diagram of the steel beam (i.e.: optimize FRP reinforcement to moment demand). The effects of bond imperfections on steel members with bonded FRP materials loaded in tension were the second topic explored in this study. It is important to determine defects or bond imperfections, due to the fact that these imperfections may ultimately control the capacity of the composite member. Finally, the use of elastic FRP strips in the compression region of the steel members was analyzed.

Sebastian and Luke (2007) provide several conclusions about the interface failure mechanics of the FRP material and the steel substrate. For the bonded FRP in tension, failure of the composite member occurred due to buckling of the member and the separation of the composite strip from the surface of the steel. In the instance of the four layered composite strip, it was found that the FRP materials exhibited interlaminar failures before separating from the steel substrate. Sebastian and Luke cite bond imperfections, localized bending of the strips, and the presence of adhesive fillets as affecting this behavior. During experimental testing, several of the beams maintained their final load through larger deflections than may be expected. This is most likely due to the redistribution of the stresses to the composite material while buckling occurred in the steel member.

Based on the strains in the FRP material, the peak available FRP-to-steel bond stress capacity was determined to be 3.55 ksi (24.5 N/mm^2). The observed bond stress is largest at the ends of the FRP material. For the FRP strip under compression, buckling failure of the strip was observed in the region of steel buckling (largest deformations) and eventually led to

15

the brittle separation of the edges of the composite in this region. Sebastian and Luke concluded that minimally invasive strain measuring techniques may aid in the further quantification of bond stresses between substrates and composite materials. Also, the fatigue performance of steel retrofitted with composite materials should be explored further to determine the full potential of composite technology.

Schnerch et al. (2005) explored the bond behavior of CFRP-strengthened steel bridge girders. This focused on uncracked steel girders, strengthened with CFRP strips. These ultra-high modulus CFRP (uhmCFRP) strips had an elastic modulus of 49,000 ksi (338 GPa) and an ultimate elongation of 0.0033; they had a linear stress-strain behavior. The test specimens utilized in this experiment were wide flanged steel members, designated SLB 100 x 4.8. The first number designates the nominal depth in millimeters and the second designates the mass in kilograms per meter. To simulate a bridge girder, a steel plate was welded to the compression flange to simulate a composite concrete deck. The CFRP composite material strips were adhered to the tension flange, each strip having a width of 1.42 in. (36 mm) and a thickness of 0.06 in. (1.45 mm). The development length provided for the CFRP strips ranged from 1.97 in. (50 mm) to 7.87 in. (200 mm). The development length was defined as "the distance from one of the load points to the end of the CFRP strip, in a region of constant shear force and decreasing bending moment towards the end of the strip." That is to say, the length of the CFRP extending into the shear span of a beam loaded in four point bending. Schnerch et al. loaded each steel specimen until a tension flange strain of 0.008 was achieved. One of two events occurred: 1) if sufficient development was provided, the CFRP ruptured at a strain near its ultimate elongation; or 2) the CFRP debonded from the steel due to insufficient development length.

When determining the most suitable adhesive for applying CFRP to a steel substrate, one must account not only for the CFRP strain at failure and the mode of failure, but also the adhesive material which can fully utilize the CFRP at the shortest development length. The shortest development length adhesives, having development lengths of 3-4 in. (76-102 mm), were Weld-On SS620 and SP Spabond 345. "The remaining adhesives had development lengths as follows: the Vantico Araldite 2015 and Jeffco 121 adhesives had a development length of 4-5 in. (102-127 mm), Fyfe Tyfo MB had a development length of 6 in. (152 mm) and Sika Sikadur 30 had a development length of more than 8 in. (203 mm). The CFRP strip strain at rupture or debonding for the tested adhesives and respective development lengths are given in Table 2.3. The development length of the CFRP strips used, independent of adhesive type, as determined by Nozaka et al. (2005), is less than 8 in. (203 mm). Schnerch et al. concluded that the bond of the FRP to the steel is largely dependent upon surface preparation of the steel.

A complete discussion of factors affecting bond to steel substrates is beyond the scope of the present work. Cadei et al. (2004) provides an overview of factors affecting FRP-to-steel bond including those associated with a) surface preparation; b) environmental exposure; c) creep and fatigue behavior; and, d) issues associated with mitigating galvanic corrosion.

2.6   FIELD APPLICATIONS OF FRP ON STEEL STRUCTURES

Several applications of FRP to steel have been used in the engineering industry to investigate and demonstrate this burgeoning technology. Moy (2004b) reports three case studies of CFRP strengthening of metallic structures on the London Underground. The first study focused on the retrofitting of a steel bridge D65A. This structure serves as a bridge for Underground trains, over a road in Acton, West London. The bridge has both main and secondary girders, where the secondary girders directly support the railway track. The loading on these secondary girders is almost entirely live loads, and fatigue is a major concern. To extend the life of the girders, the live load stresses were to be reduced by 25%. Traditionally, this would be accomplished through the addition of welded steel plates. Since, the steel plates would require extensive scaffolding; the road below the railway bridge would have to be shut down. This problem was averted, by using lighter weight CFRP material. The steel substrate was cleaned, and the CFRP plates were easily applied with epoxy. A major concern was the frequent train loading while the epoxy adhesive was curing. Testing was performed to assess the effects of cyclic loading during cure on the adhesive bonding the CFRP to the steel. After confirming the results would be adequate for the bridges' needs, CFRP plates were applied to the underside of the bridge. As a result of the CFRP application, a 24% decrease in the live load stresses was reported, accomplishing the objective of the retrofit while maintaining the road beneath the bridge open during application.

The second study reported by Moy (2004b) was vent shaft V129, in Shadwell Station, East London Line. The vent struts needed reinforcement, while allowing the trains in the tunnel below to keep running. CFRP was applied to the struts using the DML RIFT (Resin

Infusion under Flexible Tooling) technique. The struts were successfully strengthened, and no sign of deterioration was noted. Finally, a third case study focused on the tunnel support structure on the Circle Line. The strengthening of the ceiling of the tunnel was accomplished using an all CFRP beam system. These cases demonstrate the versatility of FRP composite materials in solving structural deficiencies in existing structures.

Chacon et al. (2004) studied the application of CFRP to the Ashland Bridge, in Delaware, USA. Through the application of CFRP plates to the beams of the bridge, the stiffness of the beams and distribution of applied loads was improved. The retrofit decreased the strain in the beams by 5.5%.

2.7   STRUCTURAL STABILITY OF STEEL SECTIONS

Structural stability is a significant and large area of study. In the following brief synopses, three studies which have been used to help to identify potential design spaces for the use of FRP stabilization are introduced. Nakashima et al. (2002) focused on lateral instability and lateral bracing of steel beams subjected to cyclic loading. One must first understand the behavior of steel members under such loading, before determining the impact of retrofits to aid or inhibit such behaviors. Lateral instability behavior is affected by the type of loading, whether it is cyclic or monotonic loading. Particularly when the slenderness ratio about the weak axis of a steel member is large, cyclic load behavior is degraded in comparison with monotonic load behavior; this is largely due to the extent of out-of-plane deformations. The eventual formation of a plastic "kink" (occurring at the point of largest

out-of-plane deflection) also impairs the behavior of compression members and tension-compression members such as braces (Bruneau et al., 1998). This behavior will be discussed further in Chapter 5.

Nakashima et al. (2002) developed limit curves relating web and flange slenderness to expected instability behavior. Figure 2.1 shows such a curve generated for the performance objective that the moment capacity meets or exceeds the plastic moment capacity ($M/M_p > 1.0$) at a rotation capacity of 0.045 radians. The curve shown is additionally coupled with the requirement that $L/r_y < 80$, also to ensure $M/M_p > 1.0$. Such limit curves may be drawn for any performance objective. The curves describe four distinct "regions" of behavior: *A*: behavior controlled by flange local buckling (FLB) followed by lateral torsional buckling (LTB); *B*: behavior controlled by LTB occurring almost simultaneously with FLB; *C*: behavior controlled by web local buckling (WLB) followed by almost simultaneous FLB and LTB; and, *D*: behavior controlled by web shear buckling (WSB) resulting in rapid loss of capacity upon onset of buckling due to reduction in beam depth.

LTB can be mitigated by improving bracing. As the slenderness approaches zero (i.e.: $L/r_y \rightarrow 0$), the limit curve shifts to encompass a greater range of beam geometries. Additionally, as LTB is mitigated, Region B is minimized and there is a more abrupt transition between Regions A and C. The ranges of geometric properties of typically available U.S. wide flange beam shapes are shown in Figure 2.1b. Only 49 of 146 available W-sections satisfy the performance objective shown (Nakashima et al., 2003). Additionally, most behavior is predicted to be in Regions A and B. Mitigating LTB will shift the limit curve to the right and "sharpen" the Region B transition. In such a case, more sections will

20

satisfy the performance criteria but those remaining will be dominated by the more critical Region A behavior. Thus it is demonstrated that there is a considerable design space for FRP stabilized sections to mitigate the critical FLB behavior.

Uang and Fan (2001) investigated the cyclic stability criteria for steel moment connections with a reduced beam section. Reduced beam section moment connections are growing in usage throughout the industry. These connections have a portion of the beam flange intentionally removed a short distance from the connection in order to develop a controlled plastic hinge having a capacity less than the adjacent connection, thereby "protecting" the connection from plastic deformations. This reduction in the beam flange increases the importance of lateral bracing of the steel beam member. In their experiments, 55 full-scale specimens of reduced steel beam sections were analyzed to assess the relationship between plastic rotation capacity and rate of plastic hinge strength degradation. The observed response of these sections was largely accounted for by the slenderness ratio associated with web local buckling and not the lateral-torsional buckling of the member. The failures involved controlled local flange buckling leading to crippling of the adjacent slender web; this results in a "collapse" of the section as the depth and thus plastic capacity is dramatically reduced. It was found that when the reduced beam section is placed with a composite concrete slab it only improves this behavior in positive bending region (by providing lateral bracing to the compression flange); whereas in the negative bending region, the concrete slab provided little assistance in enhancing the plastic rotation capacity of the reduced beam section.

Uang and Fan (2001) quantified the interaction between lateral torsional buckling (LTB) and flange (FLB) and web local buckling (WLB). The relationship between beam

rotation capacity and flange, web and beam slenderness ratios highlight the interaction between buckling behaviors and demonstrated a) that behavior is more sensitive to WLB behavior where it is critical; and b) that there is a relatively weak interaction with LTB in any case. Uang and Fan proposed equations to provide flange, web and beam slenderness limits based on desired rotation capacity. The reality however is that such slenderness limits are only be achievable with more expensive "built-up sections" (those fabricated from welded plates rather than rolled sections). Thus the design space for improving stability behavior through *FRP stabilization* is again demonstrated.

Okazaki et al. (2006) studied the stability requirements for beams in seismic load resisting steel moment frames. The more rotation in a steel member, the more important the effects of local buckling become. The greater the rotation demands, the smaller the flange and web width-thickness ratios must be. Local buckling or a combination of local buckling and lateral torsional buckling play a large part in the degradation of strength. When dealing with shallow wide flange beams (depth-width ratio of 2.05), and a target rotation of no greater than 0.03 radians, lateral torsional buckling is negligible. However, when dealing with deep beams (depth-width ratio of 2.84), and a target rotation of 0.04 radians, lateral torsional buckling is the controlling factor more so than the local buckling of the structural steel element. This again demonstrates the importance of the slenderness of an element and the role which lateral torsional buckling and local buckling play in the stability of a structural steel element.

2.8 ENHANCING STABILITY OF STEEL SECTIONS USING FRP

Ekiz et al. (2004) looked at the possibilities of enhancing plastic hinge behavior in steel flexural members using carbon fiber reinforced polymer (CFRP) wraps. They investigated four steel flexural specimens under reversed cyclic loading; two of the specimens were completely wrapped in CFRP in the plastic hinge region. Variables considered were the fiber orientation and the wrapping scheme on the structural steel members. One of the goals of this program was to introduce the concept of utilizing CFRP reinforcement in the plastic hinge region of steel members to aid in decreasing local slenderness and lateral torsional buckling constraints, ultimately aiding in the advancement of CFRP materials in new construction and seismic region improvements.

Ekiz et al. (2004) used two double-channel built up members, and placed CFRP wraps around the expected plastic region of the elements. After completing the reversed cyclic loading tests on the structural frame, the behavior of the unwrapped steel sections was compared to that of the CFRP-wrapped sections. The CFRP wrapping in the plastic hinge region greatly improved the behavior of the structure. It was concluded that CFRP wrapping can increase the size of plastic hinge region (thus permitting greater energy dissipation through plastic deformation), while inhibiting local buckling and delaying lateral torsional buckling. This ultimately increases the rotational capacity, improves structural fatigue behavior, and aids in the dissipation of energy throughout the plastic hinge region. From these conclusions, Ekiz et al. suggested that the use of CFRP wraps in areas of high seismic activity may be suitable for upgrading existing structures.

Accord et al. (2006) utilized nonlinear finite element analysis to examine the effects of low modulus GFRP strips bonded to I-shaped sections developing plastic hinges under moment-gradient loading. The provision of GFRP strips provided effective bracing of the flange outstands delaying the formation of local buckling of the compression flange, ultimately increasing structural ductility. Representative results from Accord et al. are shown in Figure 2.2. In this figure, the same amount of GFRP is located at different locations on the slender flange. As may be expected, the greatest improvement in behavior is affected when the GFRP is located as close to the flange tips as possible.

2.8.1 Companion Study on FRP Stabilization for Elastic Buckling (Abraham, 2006)

The present thesis represents one part of an experimental program investigating both elastic and inelastic buckling behavior of FRP stabilized members. This work reports inelastic buckling studies while Abraham (2006) discussed elastic buckling behavior. In both studies, specimen sections and retrofit details are the same and are reported in Chapter 3.

In Abraham's work, the WT 6x7 sections were cut to a length of 65.5 in. (1664 mm). A double angle connection engaging only the stem of the WT was designed to a) reflect an AISC-compliant (2005) brace connection; and b) result in a transfer of forces coincident with the neutral axis of the WT section. All specimens were heavily instrumented (similar to that reported in Chapter 3) and tested under concentric cyclic compressive loading to failure. Each brace was initially subjected to a small tensile force of approximately 2 kips (8.9 kN) to allow the loading sequence to pass through zero in each cycle. The first loading cycle imposed a maximum 5 kips (22.2 kN) compressive load and then returned to the initial 2 kips

tensile load. The following cycles incrementally increased the maximum compressive load by 5 kips each cycle and each returned to the initial 2 kips tensile load upon cycle completion. Each specimen reached at least 45 kips (200 kN) in this manner and cyclic loading was continued until failure occurred as defined by either excessive lateral deflection or FRP strip debonding.

A summary of test results and images of each specimen are shown in Table 2.4. Each specimen exhibited elastic lateral torsional buckling (LTB) typical of a slender WT section. This behavior is characterized by large lateral translations of the stem tip, twist about the centroid and nominal strong axis translation as shown in Table 2.4. For the very slender stem WT tested ($d/t_w = 29.8$), plastic 'kinking'' of the stem was observed with increased axial (and thus lateral) displacement. This behavior is particularly obvious in Specimen C (Table 2.4). The presence of FRP on subsequent specimens helped to mitigate this post-buckling crippling.

The FRP retrofit specimens did not provide a significant increase in axial capacity compared to the control specimen. The GFRP-2 and GFRP-1 retrofit specimens exhibited 6% and 9% increases in axial capacity, respectively. Specimens CFRP-2 and CFRP-1 exhibited a slight decrease in axial capacity as compared with the control specimen, possibly resulting from misalignment of the specimen in the test frame.

Despite little effect on axial capacity, the retrofit specimens did exhibit greater control over the weak-axis lateral displacement as well as the weak and strong-axis bifurcation loads. Weak-axis lateral displacement values of 0.1 in. (2.5 mm) and 0.3 in. (7.6 mm), representing mid-height lateral displacements of L/655 and L/218, respectively, are arbitrarily selected to illustrate specimen behavior. A weak-axis lateral deflection of 0.1 and

0.3 in. occurred at higher loads for the FRP-retrofitted specimens than for the control specimen. The load to cause a 0.1 in. weak-axis lateral deflection increased between 5% and 46% for the FRP-retrofitted specimens. The load to cause a 0.3 in. weak-axis lateral deflection increased between 6% and 20% for the FRP-retrofitted specimens. An increase in the weak-axis bifurcation load ranging from 5% to 13% was observed. The strong-axis bifurcation load was also observed to increase suggesting a mechanism where the FRP provides stability to the relatively unstable stem and ultimately delays the onset of strong-axis buckling of the brace member.

2.9   RELATIONSHIP TO PRESENT WORK

The research discussed in this chapter was aimed at providing some justification and background for investigating the behavior and use of FRP materials for stabilization of the plastic buckling of slender steel sections. In the following chapters, the use of FRP materials in a flanged steel section is studied to assess the ability to control the manifestation of local buckling of a steel section. A companion study (Abraham, 2006) focused on the elastic buckling behavior of FRP stabilized steel sections, whereas the focus of this work is inelastic buckling behavior.

Table 2.1 Typical properties of steel-adhesive-FRP systems. (Harries and El-Tawil, 2006)

	Mild Steel	FRP Strips				Adhesive[1]	
		hsCFRP[1]	hmCFRP[1]	uhmCFRP[1]	GFRP[2]	high modulus	low modulus[3]
tensile modulus GPa (Msi)	200 (29)	166 (24)	207 (30)	304 (44)	42 (6)	4.5 (0.65)	0.4 (0.06)
tensile strength MPa (ksi)	276-483 (40-70)	3048 (442)	2896 (420)	1448 (210)	896 (130)	25 (3.6)	4.8 (0.7)
ultimate strain, %	18-25	1.8	1.4	0.5	2.2	1.0	>10
density kg/m^3 (lb/ft^3)	7530 (490)	~1618 (~101)	~1618 (~101)	~1618 (~101)	~2146 (~134)	~1201 (~75)	~1201 (~75)
CTE 10^{-6}/^{o}C (10^{-6}/^{o}F)	21.6 (12)	~0	~0	~0	8.8 (4.9)	162 (90)	n.r.
strip thickness mm (in.)	-	1.3 (0.05)	1.3 (0.05)	1.3 (0.05)	1.5 (0.06)	-	-
strip width	-	typically up to 150 mm (6 in.)				-	-
T$_g$[4] ^{o}C (^{o}F)	-	149 (300)	149 (300)	149 (300)	resin	63 (145)	-
shear strength MPa (psi)	-	-	-	-	-	24.8 (3600)	9.0 (1300)
bond strength kPa (psi)	-	-	-	-	-	~20.7 (~3000)	~5.0 (~725)

[1] representative data from single manufacturer (SIKA Corporation); a number of companies provide similar products
[2] data from single manufacturer (Tyfo), there is only one known preformed GFRP product offered in the infrastructure market
[3] traditionally, high modulus adhesive systems are used in strengthening applications; an example of a very low modulus adhesive is provided to illustrate range of properties
[4] T$_g$ = glass transition temperature
n.r. = not reported

Table 2.2 Recommended degradation sub-factors for various FRP materials. (Moy, 2004)

Degradation Mechanism	Material partial safety sub-factor γ_{mes}					
	E-glass (GFRP)		Aramid (AFRP)		Carbon (CFRP)	
	Minimum	Maximum	Minimum	Maximum	Minimum	Maximum
Moisture	1.1	2.0	1.1	1.25	1.0	1.15
Chemical Exposure	1.0	1.33	1.0	1.15	1.0	1.15
UV Exposure	1.0	1.05	1.1	1.33	1.0	1.05
Fatigue	1.0*	4.0†	1.0*	2.5†	1.0*	2.0†
Creep	1.0	2.5	1.0	1.67	1.0	1.25
Impact	1.0	1.33	1.0	1.25	1.0	2.0
Overall Degradation	2.5	6.67	1.67	4.0	1.5	3.0

* the factor of unity applies where there is no fatigue loading
† upper bound value due to high amplitude, high frequency load cycles

Table 2.3 CFRP strip strain at rupture/debonding for tested adhesives/development lengths. (Schnerch et al., 2005)

Adhesive	Development Length					
	8 in.	6 in.	5 in.	4 in.	3 in.	2 in.
Weld-On SS620	0.00308	0.00296	-	0.00316	0.00290	0.00259
	rupture	rupture		rupture	rupture	debond
SP Spabond 345	0.00288	0.00294	-	0.00311	0.00243	0.00183
	rupture	rupture		rupture	debond	debond
Vantico Araldite 2015	0.00309	0.00298	-	0.00282	0.00277	-
	rupture	rupture		rupture	debond	
Jeffco 121	0.00298	0.00328	0.00266	0.00244	-	-
	rupture	rupture	rupture	debond		
Fyfe Tyfo MB2	0.00347	0.00306	-	0.00210	-	-
	rupture	debond		debond		
Sika Sikadur	0.00281	-	-	-	-	-
	debond					
*underlined values are the average of two test results						

Table 2.4 Elastic buckling test results. (Abraham, 2006)

Photo of specimen at end of testing					
Specimen	**C**	**CFRP-2**	**CFRP-1**	**GFRP-2**	**GFRP-1**
maximum compressive capacity (kips)	49.2	48.8	47.9	52.2	53.7
load at 0.1 in. weak axis deflection (kips)	26.1	33.3	27.4	38.0	32.4
load at 0.3 in. weak axis deflection (kips)	37.3	41.6	39.6	44.7	42.5
weak axis bifurcation load (kips)	29.7	31.5	31.0	33.5	32.6
strong axis bifurcation load (kips)	33.3	53.1	47.2	46.1	48.8

(a) example of limiting curves
for 0.045 rad.

(b) range of geometries for
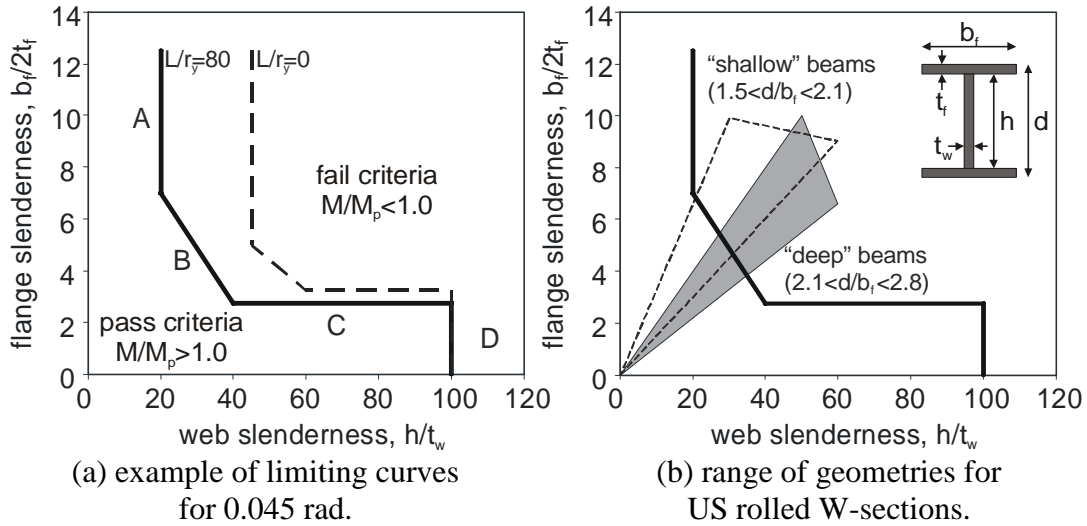US rolled W-sections.

Figure 2.1 Slenderness limits associated with beam instabilities.
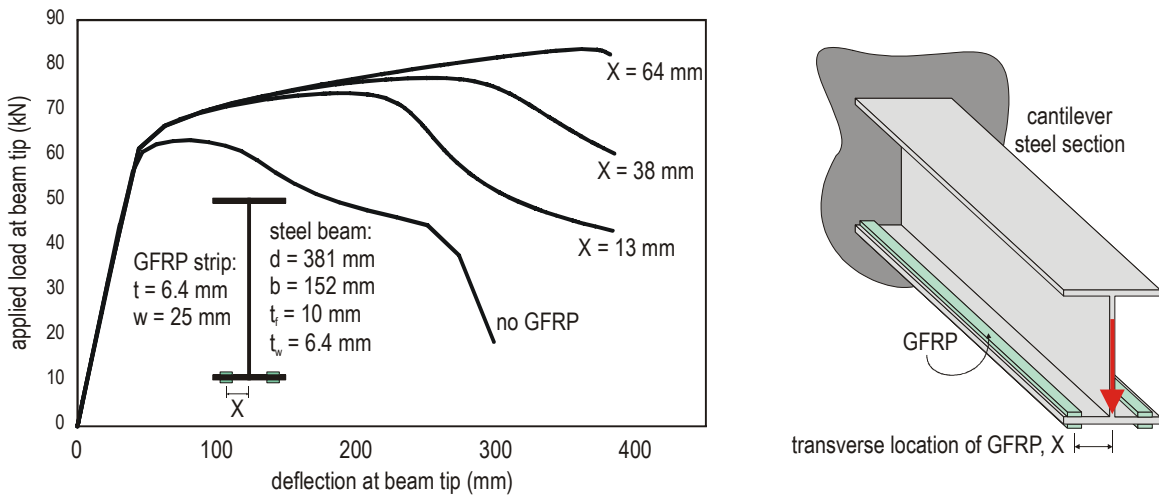(after Nakashima et al., 2003)

Figure 2.2 Analytical load-deflection behavior of GFRP stabilized steel cantilever.
(Accord et al., 2006)

3.0   EXPERIMENTAL PROGRAM

This section describes the experimental procedure including: the WT 6x7 steel sections used, fiber reinforced polymer retrofit procedures, specimen designation, experimental setup, instrumentation, experimental procedure, and the predicted WT behavior under axial compression.

3.1   WT STEEL SECTION SPECIMENS

Throughout this experimental program, ASTM A 992 Grade 50 WT 6x7 (U.S. designation) steel sections were utilized. Each specimen was cut to a length of 14 in. (356 mm). The length selected was determined after several specimens having varying lengths were tested in concentric compression (squash tests). The peak load at which each specimen buckled was recorded, and the optimal length of 14 in. (356 mm) was selected based on the desire to have a specimen dominated by local plastic buckling. The specimen lengths and their corresponding peak axial load are given in Table 3.1 and shown in Figure 3.1. A length of 14 in. clearly falls in the region dominated by local buckling (initial steeper slope in Figure 3.1) while still providing sufficient length to which to bond the FRP. The squash tests also established the squash load as being 105 kips (467 kN). The theoretical value of the squash load based on nominal material

properties is $A_g f_y$ = (2.08 in^2) (50 ksi) = 104 kips (463 kN). Figure 3.2 shows the seven trial squash test specimens.

After establishing the specimen length, different fiber reinforced polymer (FRP) stabilization configurations were designated. In addition to the control specimens, having no FRP, carbon FRP (CFRP) and glass FRP (GFRP) were utilized to stabilize the slender stem of the WT sections. The material properties of the FRP are given in Table 3.2. Two different configurations of both CFRP and GFRP were used, and are shown in Figure 3.3. Each FRP strip was 13 in. (330 mm) in length, and was laid out in one of two configurations. The designation CFRP-1 or GFRP-1 represents two 1 in. (25.4 mm) strips affixed on top of one another while CFRP-2 or GFRP-2 represents a single 2 in. (50.8 mm) strip of FRP adhered to the steel substrate. Both FRP configurations were applied such that the centroid of the FRP is located 1.5 in. (38.1 mm) from the end of the WT stem. It is noted that the cross section details and FRP and adhesive materials used are the same as those used by Abraham (2006).

3.2 FRP RETROFIT PROCEDURES

Two different FRP materials (CFRP and GFRP) having two configurations (two 1 in. strips and one 2 in. strip) were applied to the stems of WT 6x7 sections. The purpose of these FRP retrofits was to investigate the potential stabilizing effects of the FRP on the plastic buckling of the WT webs under concentric axial compression.

3.2.1 FRP Retrofit Configurations

The two types of FRP used were: Fyfe Tyfo UC high strength carbon FRP and UG ultra high modulus glass FRP. Both FRP types were affixed to the steel with Fox Industries' FX 776 epoxy adhesive. FX 776 is a two-part ambient-cure epoxy system specifically intended for use with FRP materials on steel or concrete substrates. The manufacturer reported material properties of the FRP and adhesive are given in Table 3.2. Both the CFRP and GFRP were originally provided in strips having unidirectional fiber orientation with a width of 4 in. (102 mm) and a thickness of 0.055 in. (1.4 mm) and 0.075 in. (1.9 mm) for the CFRP and GFRP, respectively. From these strips, the specimen strips were cut. Two different configurations for both CFRP and GFRP were used as shown in Figure 3.3. Both FRP configurations were applied such that the centroid of the FRP is located 1.5 in. (38.1 mm) from the end of the WT stem. Each 13 in. FRP strip was laid out in one of two configurations: Specimens CFRP-1 and GFRP-1 consist of two 1 in. (25.4 mm) strips affixed on top of one another. This was achieved by first adhering the two strips together using FX 776 adhesive. This double-thickness strip was allowed to cure in ambient conditions for 24 hours before being adhered to the WT stem, again using FX 776 adhesive. The single 2 in. (50.8 mm) wide strips of the CFRP-2 and GFRP-2 specimens were applied directly to the WT stem following surface preparation as described below. Both FRP configurations had the same amount of FRP material. Three specimens of each FRP and configuration were prepared resulting in a total of 15 specimens.

3.2.2 Application of FRP to Steel Specimens

To ensure the quality of the bond between the FRP and the steel substrate, the following procedures were followed.

3.2.2.1 Preparation of Steel Substrate

All steel specimens were cut to a length of 14 in. (356 mm). After the steel was cut to length, both cross sectional faces of the steel were faced using a belt sander to ensure parallel end bearing faces. This was done to ensure a uniform distribution of bearing forces across the entire section.

To achieve maximum bonding effectiveness, the steel surface to which the FRP was to be applied required preparation so that a clean bare steel surface was achieved. To accomplish this, a 40 grit zirconia alumina sanding belt was used to clean and roughen the stem of the WT surface (see Figure 3.4). Immediately after sanding the steel specimens, an anti-corrosion agent was applied to the surface to ensure no rust would form between the time the steel was sanded and the FRP was applied. This clean surface was maintained until FRP application by placing all steel specimens in a dry and clean environment.

3.2.2.2 Preparation of FRP

A 13 in. (330 mm) length of FRP was chosen as this maximized the available development length on the 14 in. (356 mm) stem. The effective bond length in. for the CFRP and GFRP strips used is calculated as given in Equation 3.1 (Nozaka et al. 2005). The effective bond length, L_e, is the length of FRP beyond which an increase in bonded length no longer results in an increase in bond capacity. This length is somewhat analogous to the development length of a reinforcing bar in concrete.

$$L_e = 4.6 \left/ \sqrt{\frac{G_a}{t_a}\left(\frac{1}{E_s t_s} + \frac{1}{E_{FRP} t_{FRP}}\right)} \right. \qquad \text{(SI units)} \qquad\qquad 3.1$$

Where, E_s, E_{FRP}, t_s, t_{FRP} are the Young's modulus (MPa) and thickness (mm) of the steel and FRP. G_a and t_a are the shear modulus (MPa) and thickness (mm) of the adhesive layer. L_e is estimated to fall between 1.2 and 1.6 in. (30-40 mm) for the GFRP used and between 2.4 and 3.0 in. (60-75 mm) for the CFRP used. In both cases, the 13 in. length of FRP permits the development of the required effective bond length on both sides of the midheight region.

Both CFRP and GFRP were cut to the specified length using a variable speed dremel abrasive wheel cut-off tool. Since both the carbon and glass FRP come in 4 in. (101.6 mm) wide strips, all FRP material was cut to the specified width of either 1 in. (25.4 mm) or 2 in. (50.8 mm) using a razor blade. Once the FRP was cut to width, both surfaces of the FRP were cleaned with isopropyl rubbing alcohol. This was done to ensure a clean application surface. This clean surface was maintained until application by placing all FRP specimens in a dry and clean environment.

The FRP configurations involved both a single 2 in. (50.8 mm) FRP strip and two 1 in. (25.4 mm) FRP strips applied on top of one another. For the 1 in. (25.4 mm) FRP "sandwiched" strips, one strip was applied directly on top of the other using the FX 776 adhesive. Uniform pressure was applied to the strip to establish a thin and uniform bond line along the length of the strip and to remove air pockets that may occur within the adhesive layer. Masking tape was applied to the exterior surface of the FRP strips, to ensure a clean surface for the eventual application of strain gages. The dual layered FRP configuration was allowed to set for 24 hours before being applied to the steel specimen. The single 2 in. (50.8 mm) wide strips of the CFRP-2 and GFRP-2 specimens were applied directly to the WT stem following surface preparation.

3.2.2.3 Application of FRP to Steel Substrate

All steel specimens were placed on a clean level surface and were allowed to rest with one face of the stem on the table surface. Both the centerlines of the FRP and the steel were marked at 1½ in. (38.1 mm) from the edge of the stem as shown in Figure 3.3. The FX 776 adhesive was mixed per the manufacturer's specifications and a uniform layer of epoxy was applied to both the FRP and steel substrate. The FRP was then aligned on the steel and uniform pressure was applied to mitigate both non-uniform adhesion and air bubbles which may be present in the epoxy. The FRP was applied to the steel rapidly, so that application was complete well with the adhesive's reported pot life of about 30 minutes. The first application was permitted to cure in ambient conditions for 24 hours

and then the steel specimens were flipped and the process was repeated on the other side of the stem.

3.3   SPECIMEN NAMING CONVENTION

The specimen naming convention is as follows:

*x*FRP-*y*-*zz*

Where: x = C = Carbon Fiber Reinforced Polymer (CFRP)

x = G = Glass Fiber Reinforced Polymer (GFRP)

y = 1 = Two 1 in. (25.4 mm) wide strips

y = 2 = One 2 in. (50.8 mm) wide strip

Finally, the last number, *zz*, designates the percentage of the peak load to which the post-peak testing of the specimen was taken before stopping the test. For example, if zz = 80, the test was stopped once the peak load had fallen 20%

zz = 50 = post-peak test stopped at 50% of the peak load

zz = 80 = post-peak test stopped at 80% of the peak load

zz = 90 = post-peak test stopped at 90% of the peak load

3.4 EXPERIMENTAL SETUP

All specimens were subjected to concentric axial compression aligned through the centroid of the WT section. The axial load was applied using a 200 kip (890 kN) capacity Baldwin Universal Testing Machine (UTM). Although the WT stub columns were "ground to bear", 22 gage steel plates were placed on both the top and bottom of the specimens in order to ensure uniform distribution of force into the WT section. The lower loading surface was a flat steel cylinder 10 in. (254 mm) in diameter, while the upper plate was a similar plate backed by an 8" (202 mm) "ball joint". Thus the loading plates were larger than the WT section and may be assumed to distribute a uniform compressive force across the entire cross section. All specimens were placed in the machine as shown in Figure 3.5. Applied load is recorded through the Baldwin load cell while vertical displacement is recorded using a draw wire transducer (DWT) located between machine heads (on right of Figure 3.5). It is recognized that the DWT, in addition to recording specimen shortening, also captures seating of the ball joint, crushing of the 22 gage shim plates (considered negligible) and shortening of the load plates (also negligible). The seating of the ball joint occurs at very low applied loads and is easily corrected in the acquired data.

3.5 INSTRUMENTATION

All specimen instrumentation was similar to that used by Abraham (2006). The basic configuration of electrical resistance strain gages deployed in the steel and FRP is displayed in Figure 3.6. In the case of the control specimens, 6 strain gages were placed at the mid height of the specimens. Based on the numbering scheme in Figure 3.6, the control specimens utilized strain gages 1 through 6. All of these strain gages were centered at the same distance from the edge of the flange or stem: 0.2 in. (5.08 mm). For the FRP specimens, only the web gages were used therefore, these specimens used gages 1 and 2 on the steel and 7 and 8 on the FRP. The strain gages placed on the FRP (7 and 8) were centered along the midline of the FRP strip and were therefore 1.5 in. (38.1 mm) from the stem tip. The axial and lateral displacements were recorded using draw wire transducers (DWT). The axial displacement DWT was connected directly to the crosshead, whereas the lateral displacement DWT was clipped to the tip of the stem at the mid height of the specimen. Both DWT configurations can be seen in Figure 3.6.

All instrumentation and the Baldwin load cell were connected to a Vishay System 5100 data acquisition system. The applied loading of the specimens in the Baldwin UTM was controlled manually, at a constant rate of 100 pounds (445 N) per second, with hydraulic load controls.

3.6   EXPERIMENTAL PROCEDURE

There were a total of fifteen specimens tested in this program, three of each specimen configuration. As described earlier, each specimen configuration was loaded beyond its peak load to a percentage (50%, 80%, or 90%) of that load at which time the test was stopped. This was done to permit assessment of the buckling deformations with each FRP configuration. For each specimen, the axial load was applied at a constant rate of 100 pounds (445 N) per second. Once the peak load of the specimen was achieved, testing continued until the final target load (50%, 80% or 90% of the peak load) was reached. Finally, the specimen was unloaded at a constant rate. Following unloading and photographing, the specimen was reloaded until FRP failure occurred (if it had not done so already).

3.7   PREDICTED WT 6x7 BEHAVIOR

Steel member sections are categorized as compact, noncompact, or slender-elements based upon limiting width-thickness ratios of webs and flanges (AISC 2005). To determine the classification of the WT 6x7 sections, the limiting width-thickness ratios were calculated, as shown in Table 3.3.

AISC (2005) states, "For a section to be compact, all of its compression elements must have width-thickness ratios equal to or smaller than the limiting λ_p." The second limiting width-thickness ratio, λ_r, is the division between noncompact and slender

39

sections. Elastic local buckling is not the governing limit state for a compression element provided the limiting (web or flange) width-thickness ratio of the element does not exceed λ_r. When λ_r is exceeded, the elastic buckling strength of the compression member must be taken into account. In the case of the WT 6x7 sections used in the present work, the flanges are compact while the stem is slender:

$$\lambda_{stem} = d/t_w = 5.96/0.2 = 29.8 > 1.03\sqrt{E/F_y} = 24.8 \qquad \text{3.2 (AISC Eq. E7-15)}$$

The reduction factor for a slender unstiffened element, Q_s, is calculated based on the AISC *Specification* (2005) Section E7.1:

$$Q_s = \frac{0.69E}{F_y\left(\dfrac{d}{t_w}\right)^2} = \frac{0.69(29000)}{50\left(\dfrac{5.96}{0.200}\right)^2} = 0.451 \qquad \text{3.3 (AISC Eq. E7-15)}$$

Using this reduction factor, the local critical buckling load is determined:

$$F_{cr} = Q\left[0.658^{\frac{QF_y}{F_e}}\right]F_y = 0.451\left[0.658^{\frac{(0.451)(50)}{828}}\right]50 = 22.3\,\text{kips} \qquad \text{3.4 (AISC Eq. E7-2)}$$

Where F_e is the elastic critical buckling stress (Euler buckling stress):

$$F_e = \frac{\pi^2 E}{\left(\dfrac{kL}{r_y}\right)^2} = \frac{\pi^2(29000)}{\left(\dfrac{(1.0)(14)}{0.753}\right)^2} = 828\,\text{ksi} \qquad \text{3.5 (AISC Eq. E3-4)}$$

Finally, the calculation of the local critical buckling load of a 14 in. (356 mm) long WT 6x7 section accounting for the stem buckling limit state is found to be 46 kips (209 kN):

$$P_n = F_{cr}A_g = (22.278)(2.08) = 46.3\,\text{kips} \qquad \text{3.6 (AISC Eq. E7-1)}$$

Table 3.1 Preliminary squash test results.

Nominal Length	Peak Axial Load
2 in. (51 mm)	105000 lbs (467 kN)
4 in. (101.6 mm)	96500 lbs (429 kN)
6 in. (152.4 mm)	90500 lbs (403 kN)
12 in. (304.8 mm)	77900 lbs (347 kN)
14 in. (355.6 mm)	70600 lbs (314 kN)
18 in. (457.2 mm)	59100 lbs (263 kN)
49.5 in.[1] (1257.3 mm)	49255 lbs (219 kN)

[1] Abraham 2006

Table 3.2 Material properties reported by manufacturer.

Material	Tensile Strength	Tensile Modulus ksi (MPa)	Thickness in. (mm)	Rupture Strain
WT 6x7 Section	50 ksi (345 MPa)	29000 ksi (200000 MPa)	$t_w = 0.200$ (5.1)	-
HS Carbon FRP	405 ksi (2792 MPa)	22500 ksi (155000 MPa)	0.055 (1.4)	0.018
UHM Glass FRP	130 ksi (896 MPa)	6000 ksi (41000 MPa)	0.075 (1.9)	0.022
Adhesive	4.5 ksi (31 MPa)	575[1] ksi (4000 MPa)	0.03 (0.76)[2]	0.025

[1] tangent modulus of elasticity
[2] estimated

Table 3.3 Limiting Width-Thickness Ratios for WT 6x7.

Description of Element	Width-Thickness Ratio WT 6x7	Limiting Width Thickness Ratios		Slender Element Compression Member
		λ_p (compact)	λ_r (noncompact)	
Flexure in flanges of tees	$b/2t_f$ **8.8**	$0.38\sqrt{E/F_y}$ **9.2**	$1.00\sqrt{E/F_y}$ **24.1**	$1.03\sqrt{E/F_y}$ **24.8**
Uniform compression in stems of tees	d/t_w **29.8**	NA	$0.75\sqrt{E/F_y}$ **18.1**	$1.03\sqrt{E/F_y}$ **24.8**

Note: Equations presented in English units format
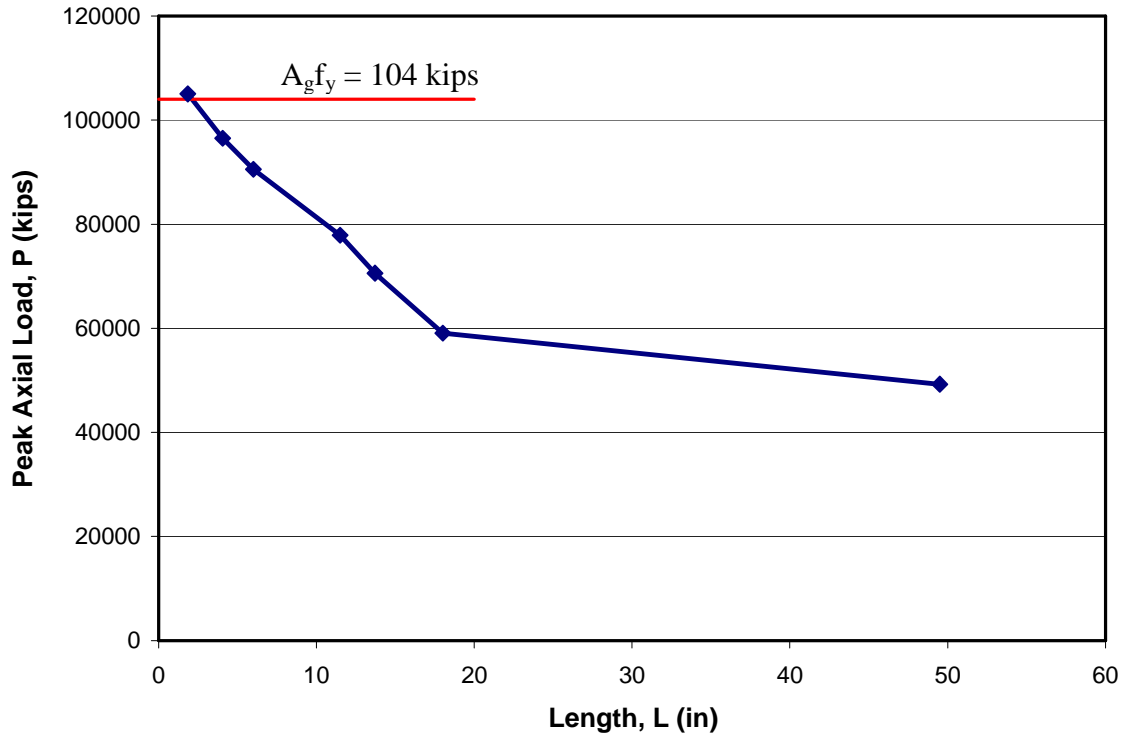
Figure 3.1 Peak axial load verses specimen length for squash tests.
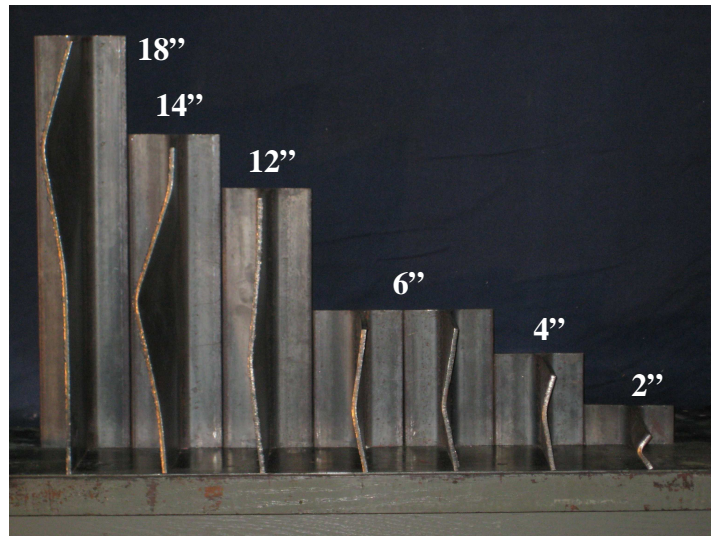
Figure 3.2 Photograph of squash test specimens.
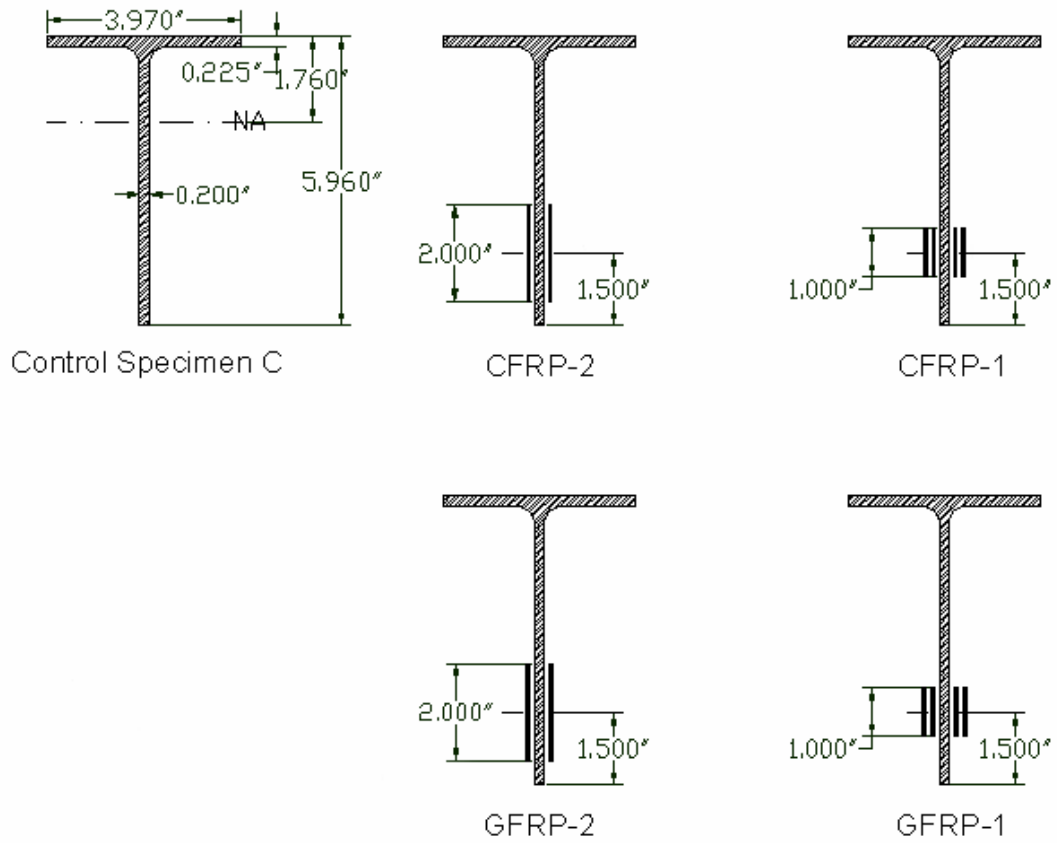
Figure 3.3 Specimen section details.

Figure 3.4 Representative photo of steel surface prepared for FRP application.
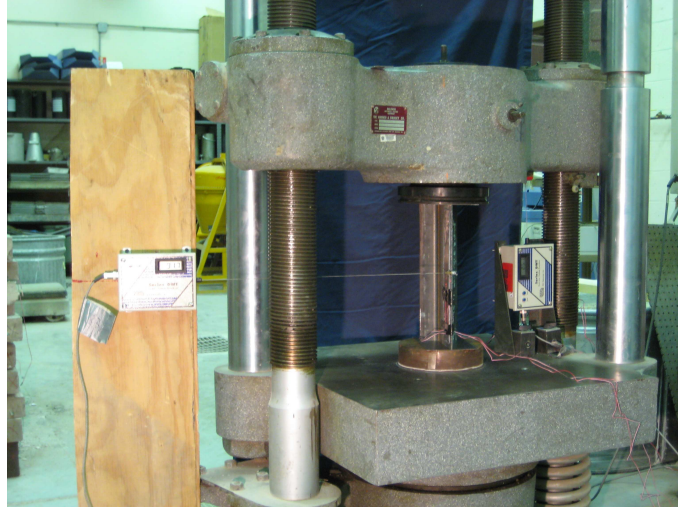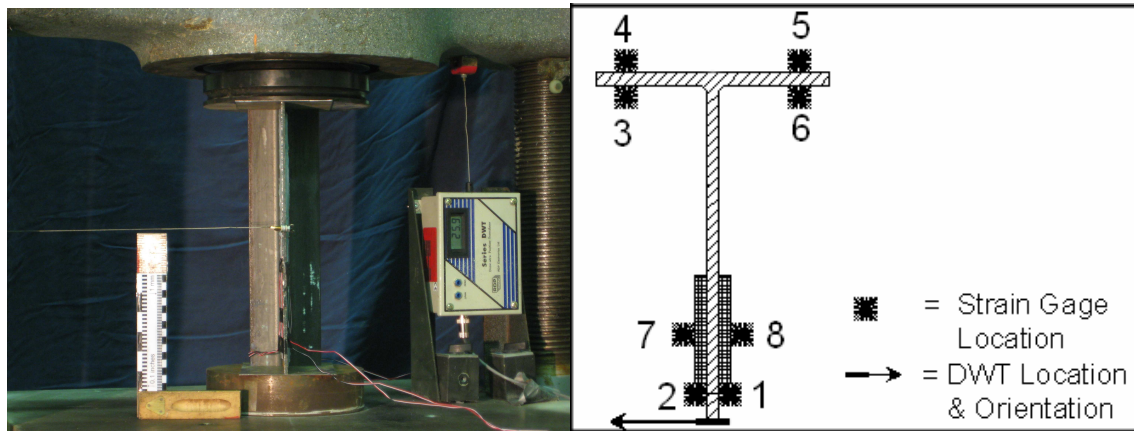
Figure 3.5 Experimental setup.

Figure 3.6 Instrumentation photo and cross sectional diagram.

4.0   EXPERIMENTAL RESULTS

This section deals with the experimental behaviors and results of each plastic buckling test of the WT 6x7 specimens.

4.1   TEST RESULTS

Table 4.1 summarizes all of the specimens' maximum axial compressive loads, axial displacements, and midheight lateral displacements. Table 4.2 displays all of the maximum strains recorded for each strain gage for each specimen. Figures 4.1 through 4.3 display both the displacement and load-strain curves of each control specimen. The displacement curve displays both the axial and lateral displacements recorded by the vertical and horizontal draw wire transducers, respectively. The three remaining graphs display the results of the strain gages throughout the testing of the specimens. A representative photograph of each control specimen accompanies the displacement curve, while a diagram of the strain gage layout accompanies the load-strain curves. Figures 4.4 through 4.15 display both the displacement and load-strain curves for each FRP specimen tested. Accompanying these curves are representative photos of the specimen at their post-peak response at an axial load corresponding to the designated percentage of the peak load (i.e.: 50%, 80% or 90%). Figures 4.16 to 4.21 show photographs of selected

test specimens at their peak and ultimate capacities. Figure 4.22 displays a bar graph of the maximum lateral displacements at midheight including representative photographs of the specimens at both 80% and 90% of the axial load capacity.

4.2   SPECIMEN BEHAVIOR

Web local buckling of the stem dominated the behavior of each test specimen. Neither flange local buckling nor lateral torsional buckling was observed in the test specimens. As indicated in Table 4.1, the presence of the FRP affected the responses to some degree. The Control specimens were additionally used to assess the test set-up and specifically to ensure that the WT sections were subject to a uniform axial load over their entire section. The following sections describe the behavior of each specimen type tested in this experimental program.

4.2.1 Axial Load Distribution and Apparent Loading Eccentricity

Table 4.3 displays the strain readings for all three control specimens at specified load intervals that were recorded during the experimental procedure. This illustrates the uniform compressive strains in the cross section at lower loads, and gives an indication when instability is initiated in the section. When one of the coupled strain gages begins recording a greater or lesser rate of change in strain, the section is displaying signs of instability.

When dealing with lower axial loads on a member under elastic behavior, the strains across a cross section should be uniform. Any non-uniform strain reading displays imperfections and/or eccentricities within the section or applied loading, causing flexural behavior. These non-uniform readings may lead to a decrease in the buckling capacity of the member. Several reasons could account for these non-uniform strain readings, such as: member fabrication, misalignment of the member in the test frame, inconsistencies within the material, or a combination of these reasons. For all of these reasons, the results achieved in this experiment may be slightly modified if any misalignment is calculated. To determine this eccentricity from the theoretical member cross sectional centroid, the strain gage data must be utilized. The strain data was taken at 10000 lbs (44.4 kN) for each member. From the strain data, and assuming the strain varied linearly throughout the member, the approximation of the strain values was determined. These strain approximations were converted to stresses and the resultant force and magnitude were determined by summing the moment about an arbitrary point. Table 4.4 displays the theoretical centroid of the WT 6x7 sections, and the calculated experimental centroids based upon the recorded strain gage data. The expected theoretical centroid based upon AISC Manual 13th Edition is located at 1.760 in. (44.7 mm) from the outside of the flange and in the middle of the stem at 1.985 in. (50.4 mm). The calculations of the coordinates of the equivalent load eccentricity displayed in Table 4.4 are displayed in Appendix A. As was observed by Abraham (2006) the x-eccentricity is on the order of 0.4 in. (10 mm) from the theoretical centroid. This is believed to result from differences between the WT sections tested and the theoretical geometry reported by AISC. The y-eccentricity is

approximately 0.1 in. (2.5 mm) in each case, possibly indicating an eccentricity in the test frame loading.

4.2.2 Control Specimen

The maximum peak axial compression load obtained from the three control specimens was 80341 lbs (357 kN). The maximum axial and lateral displacements obtained when the specimen was loaded to an ultimate load of 50% of the peak load obtained were 0.293 in. (7.44 mm) and 2.007 in. (50.98 mm) respectively. The control specimens all exhibited a significant "kink" in the web of the WT section as they buckled as clearly seen in Figure 4.16(c). This kink was less pronounced or mitigated completely, resulting in a sinusoidal buckle having no kink (for example, compare with Figure 4.20(c)) in the specimens that had FRP material applied to the web. A summary of the maximum strains recorded may be found in Table 4.2. Figure 4.16 shows representative photos of specimen Control 50.

4.2.3 Specimen CFRP-1

The maximum peak axial compression load obtained from the three CFRP-1 specimens was 89317 lbs (397 kN). The maximum axial and lateral displacements obtained when the specimen was loaded to an ultimate load of 50% of the peak load were 0.142 in. (3.607 mm) and 1.242 in. (31.547 mm), respectively. CFRP-1-50 and CFRP-1-80 specimens exhibited CFRP strip debonding initiating at one end of the CFRP strips

located on the "tension" side of the buckled web as can be seen in Figure 4.17(c). This debonding occurred after the maximum axial load was obtained and therefore was driven by the buckling-induced deformation of the web. Specimen CFRP-1-90 did not exhibit debonding (Figure 4.17(d)) indicating that the limited lateral deflection at a load of 90% of the peak load was insufficient to cause debonding in this case. It is also evident by contrasting the ultimate behavior of CFRP-1-50 and CFRP-1-90 in Figures 4.17 (c) and (d), respectively, that the formation of the kink (evident in 4.17(c)) appears to occur following debonding; this will be discussed further in Chapter 5. Of all the specimens tested, the CFRP-1 group displayed the greatest increase in the maximum axial compression value. A summary of the maximum strains recorded may be found in Table 4.2. Figure 4.17 shows representative photos of CFRP-1-50 and CFRP-1-90.

4.2.4 Specimen CFRP-2

The maximum peak axial compression load obtained from the three CFRP-2 specimens was 86406 lbs (384 kN). The maximum axial and lateral displacements obtained when the specimen was loaded to an ultimate load of 50% of the peak load were 0.253 in. (6.426 mm) and 1.537 in. (39.040 mm) respectively. CFRP-2-50 exhibited debonding at one end of the CFRP strip located on the "tension" side of the web buckle as shown in Figure 4.18(c). This debonding occurred after the maximum axial load was obtained. CFRP-2-80 did not exhibit debonding. Specimen CFRP-2-90 exhibited unique behavior: a compressive failure of the CFRP strip on the "compression" side of the buckled web was observed as shown in Figure 4.19. It is noted that the "tension" side

debonding shown in Figure 4.19 occurred after 90% of the peak load was attained; the specimen was loaded further to investigate the compressive behavior observed. The compressive failure of the CFRP in this case indicates an extremely sound bond between the CFRP and the steel. A summary of the maximum strains recorded may be found in Table 4.2. Figure 4.18 displays the representative photos of Specimen CFRP-2-50.

4.2.5 Specimen GFRP-1

The maximum peak axial compression load obtained from the three GFRP-1 specimens was 88957 lbs (396 kN). The maximum axial and lateral displacements obtained when the specimen was loaded to an ultimate load of 50% of the peak load were 0.201 in. (5.105 mm) and 1.746 in. (44.348 mm) respectively. Like the previous specimens, GFRP-1-50 exhibited debonding initiating at the end of the GFRP strip on the "tension" side of the buckled web. GFRP-1-80 and GFRP-1-90 exhibited no such debonding. A summary of the maximum strains recorded may be found in Table 4.2. Figure 4.20 shows representative photos of Specimen GFRP-1-50.

4.2.6 Specimen GFRP-2

The maximum peak axial compression load obtained from the three GFRP-2 specimens was 83476 lbs (371 kN). The maximum axial and lateral displacements obtained when the specimen was loaded to an ultimate load of 50% of the peak load were 0.260 in. (6.604 mm) and 1.438 in. (36.525 mm) respectively. GFRP-2-50 and GFRP-2-

80 exhibited debonding at the ends of the GFRP strips located on the "tension" side of the web buckle. GFRP-1-90 exhibited no such debonding. A summary of the maximum strains recorded may be found in Table 4.2. Figure 4.21 shows representative photos of Specimen GFRP-2-50.

4.3   OBSERVED DEBONDING BEHAVIOR

Table 4.5 summarizes the maximum strains recorded on the CFRP or GFRP strips in each test. The degree of through-web flexure is very evident in these values. The maximum strains attained prior to debonding are comparable to those observed in test programs of FRP adhesively bonded to either steel or concrete. The strains are also well below the reported rupture strain of the materials (See Table 3.2). One factor affecting the debonding behavior and the inability to develop FRP rupture is the relatively short bonded length used. This is discussed in Section 3.2.2.

Table 4.1 Summary of displacements resulting from axial compression.

Specimen	Maximum Compressive Load, lbs (kN)	Maximum Axial Displacement, in. (mm)	Maximum Lateral Displacement at Midheight, in. (mm)
Control 50	80341 (357)	0.293 (7.442)	2.007 (50.978)
Control 80	77727 (346)	0.111 (2.819)	0.569 (14.453)
Control 90	74398 (331)	0.163 (4.140)	0.411 (10.439)
CFRP-1-50	86419 (384)	0.142 (3.607)	1.242 (31.547)
CFRP-1-80	88621 (394)	0.080 (2.032)	0.555 (14.097)
CFRP-1-90	89317 (397)	0.081 (2.057)	0.499 (12.675)
CFRP-2-50	82742 (368)	0.253 (6.426)	1.537 (39.040)
CFRP-2-80	86406 (384)	0.108 (2.743)	0.705 (17.907)
CFRP-2-90	80105 (356)	0.082 (2.083)	0.628 (15.951)
GFRP-1-50	83247 (370)	0.201 (5.105)	1.746 (44.348)
GFRP-1-80	88957 (396)	0.072 (1.829)	0.668 (16.967)
GFRP-1-90	82205 (366)	0.080 (2.032)	0.542 (13.767)
GFRP-2-50	80966 (360)	0.260 (6.604)	1.438 (36.525)
GFRP-2-80	83476 (371)	0.082 (2.083)	0.686 (17.424)
GFRP-2-90	76898 (342)	0.109 (2.769)	0.634 (16.104)

Table 4.2 Summary of maximum strain gage readings.

Specimen	Gage 1 (µe)	Gage 2 (µe)	Gage 3 (µe)	Gage 4 (µe)	Gage 5 (µe)	Gage 6 (µe)	Gage 7 (µe)	Gage 8 (µe)
Control 50	-1339	-4398	-6663	-1530	-1350	-2871	---	---
Control 80	-4341	-1068	-1879	-1149	-1678	-1500	---	---
Control 90	-3772	-1331	-1855	-1196	-3463	-1216	---	---
CFRP-1-50	-4211	1615					3678	-6757
CFRP-1-80	-3725	920					2252	-4056
CFRP-1-90	-3830	1241					2884	-6082
CFRP-2-50	-5388	3334					5035	-7996
CFRP-2-80	-4635	2322					3066	-5419
CFRP-2-90	-4108	2273					2803	-4815
GFRP-1-50	-4347	3017					3380	-5894
GFRP-1-80	-4198	1372					4495	-2200
GFRP-1-90	-4158	1146					3962	-6891
GFRP-2-50	-5206	3392					6456	-9338
GFRP-2-80	1637	-3949					-6131	2948
GFRP-2-90	-3855	1396					2629	-5151

= Strain Gage Location
= DWT Location & Orientation
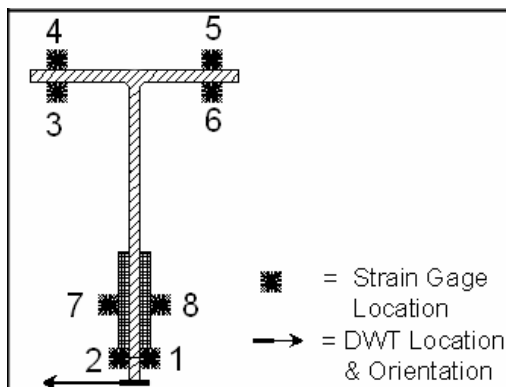
Table 4.3 Strains at applied load intervals for all 3 control specimens.

Applied Load	Gage 1 (με)	Gage 2 (με)	Gage 3 (με)	Gage 4 (με)	Gage 5 (με)	Gage 6 (με)
Control 50						
5000 lbs	-158	-148	-11	-7	-122	-116
10000 lbs	-245	-232	-89	-85	-197	-192
20000 lbs	-424	-405	-253	-247	-360	-358
30000 lbs	-597	-571	-423	-414	-524	-524
40000 lbs	-767	-729	-591	-580	-696	-700
50000 lbs	-935	-884	-755	-741	-873	-880
60000 lbs	-1101	-1037	-918	-900	-1051	-1061
70000 lbs	-1273	-1206	-1082	-1064	-1235	-1252
Control 80						
5000 lbs	-146	-134	-91	-88	-90	-92
10000 lbs	-262	-239	-195	-192	-166	-170
20000 lbs	-399	-356	-360	-355	-270	-273
30000 lbs	-558	-483	-525	-514	-449	-450
40000 lbs	-745	-625	-683	-664	-634	-632
50000 lbs	-945	-767	-839	-811	-818	-812
60000 lbs	-1156	-895	-999	-957	-1004	-991
70000 lbs	-1646	-1056	-1209	-1099	-1238	-1198
Control 90						
5000 lbs	-177	-162	-72	-66	-29	-30
10000 lbs	-320	-291	-164	-157	-60	-60
20000 lbs	-548	-497	-421	-410	-105	-101
30000 lbs	-746	-683	-649	-639	-199	-190
40000 lbs	-929	-840	-822	-805	-368	-356
50000 lbs	-1170	-1023	-992	-966	-550	-532
60000 lbs	-1566	-1244	-1178	-1120	-760	-731
70000 lbs	-2450	-1218	-1391	-1184	-1101	-957

Table 4.4 Coordinates of equivalent load eccentricity.

	x (in.)	Δx (e_x) (in.)	y (in.)	Δy (e_y) (in.)	Peak Observed Load (lbs)
Theoretical Centroid	**1.760**	---	**1.985**	---	---
Control	2.551	0.791	1.970	-0.015	80341
CFRP-1	2.074	0.314	1.890	-0.095	89317
CFRP-2	2.162	0.402	1.895	-0.090	86406
GFRP-1	2.135	0.375	1.894	-0.091	88957
GFRP-2	2.153	0.393	1.894	-0.091	83476

Table 4.5 Maximum strain gage readings on the FRP.

Specimen	Max Strain on tension side of stem (µe)	Max Strain on compression side of stem (µe)
Control 50	---	---
Control 80	---	---
Control 90	---	---
CFRP-1-50	3678	-6757
CFRP-1-80	2252	-4056
CFRP-1-90	4118	-7269
CFRP-2-50	5035	-7996
CFRP-2-80	3066	-5419
CFRP-2-90	2834	-6970
GFRP-1-50	3380	-5894
GFRP-1-80	4562	-2234
GFRP-1-90	4061	-7847
GFRP-2-50	6456	-9338
GFRP-2-80[1]	2948	-6131
GFRP-2-90	7010	-8960

[1] in all cases but GFRP-2-80, the tension side of the stem was recorded by gage 7 and the compression side by gage 8. In GFRP-2-80 this is reversed (i.e.: the web buckled in the other direction)
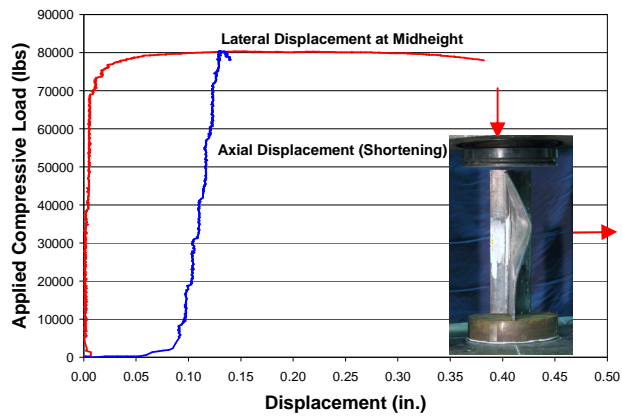
(a) Load-Displacement curves.
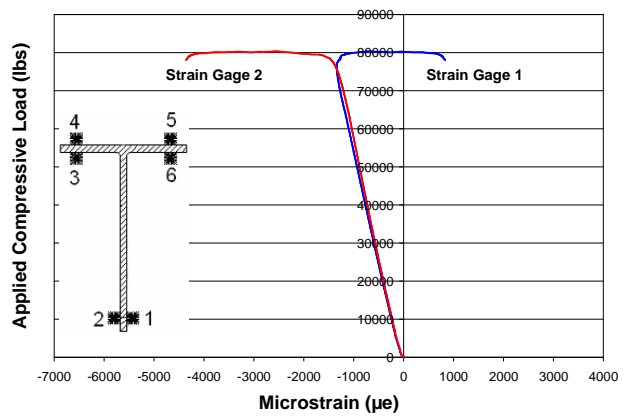
(b) Load-Strain curves.
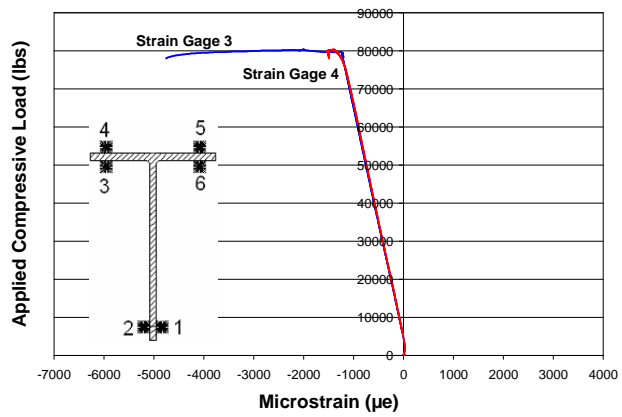
(c) Load-Strain curves.
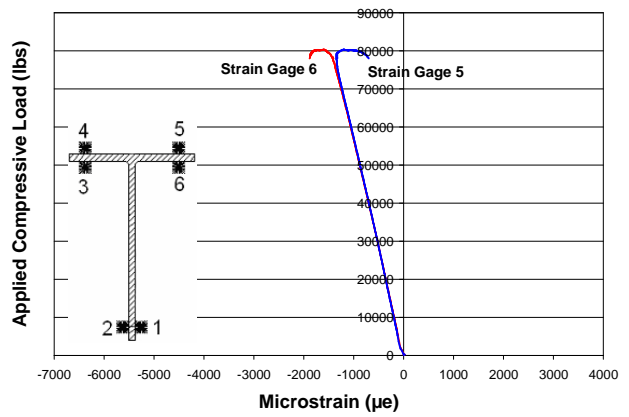
(d) Load-Strain curves.

Figure 4.1 Representative behavior of Control Specimen 50.
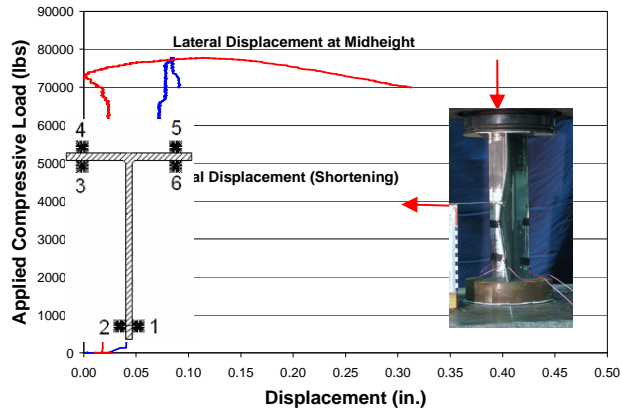
(a) Load-Displacement curves.
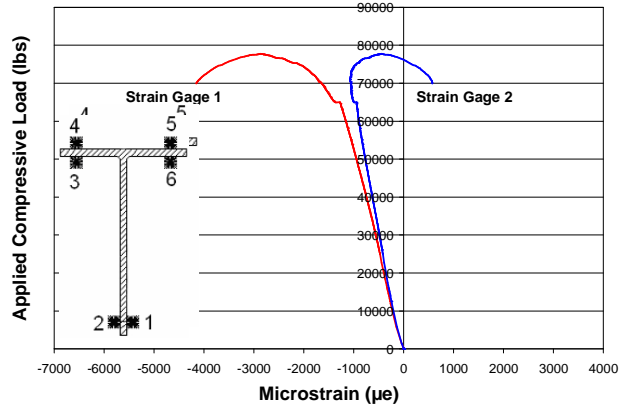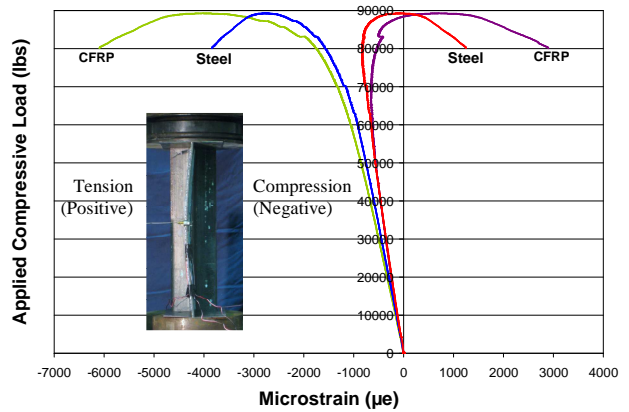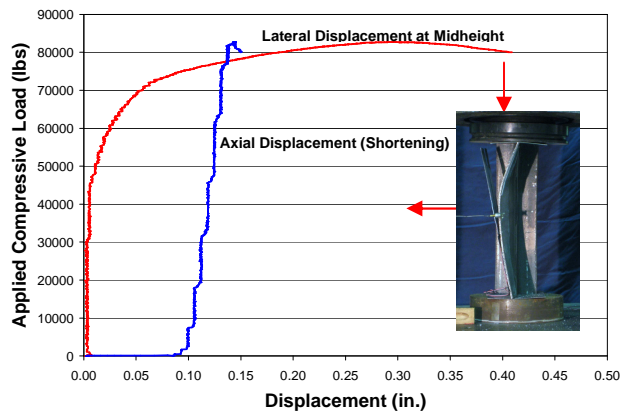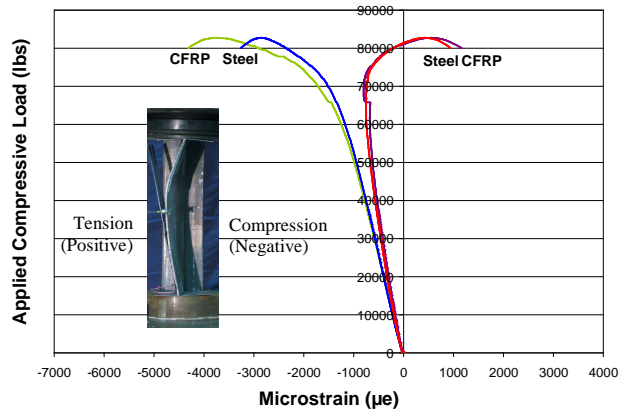
(b) Load-Strain curves.
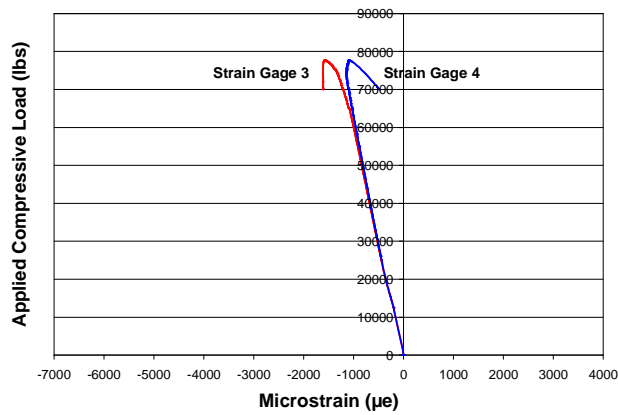
(c) Load-Strain curves.
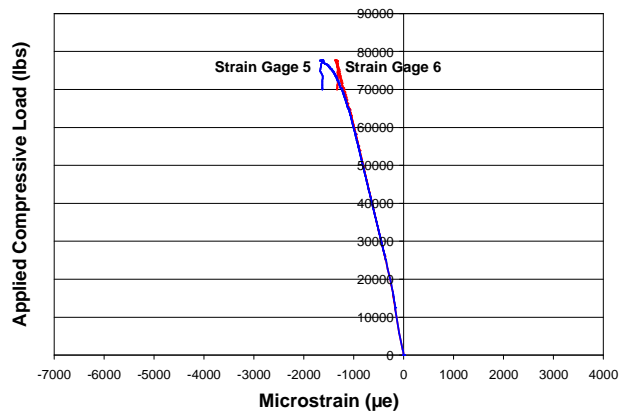
(d) Load-Strain curves.

Figure 4.2 Representative behavior of Control Specimen 80.
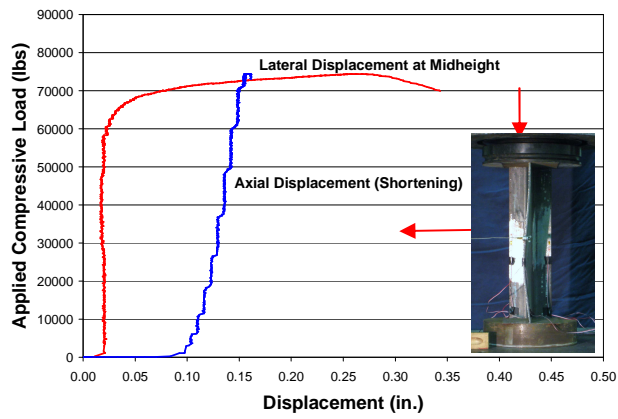
(a) Load-Displacement curves.
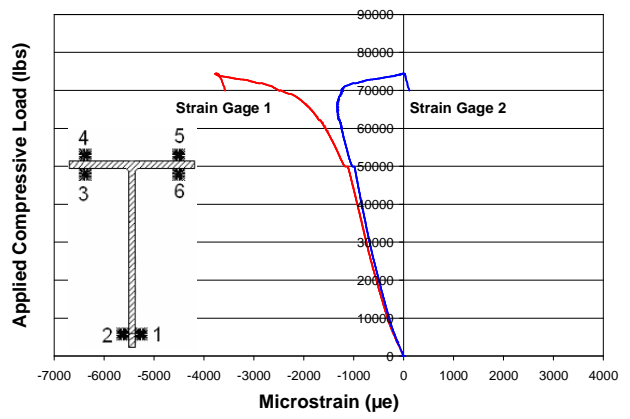
(b) Load-Strain curves.
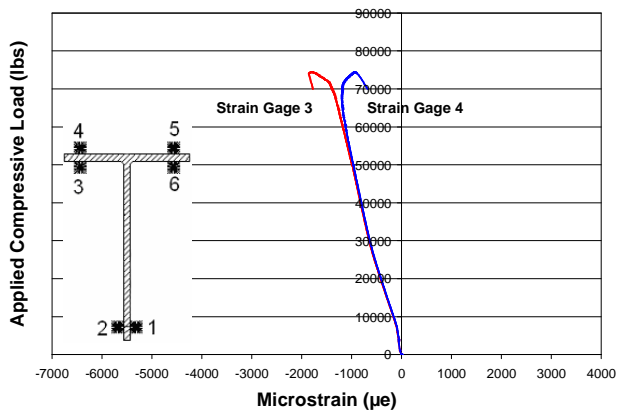
(c) Load-Strain curves.
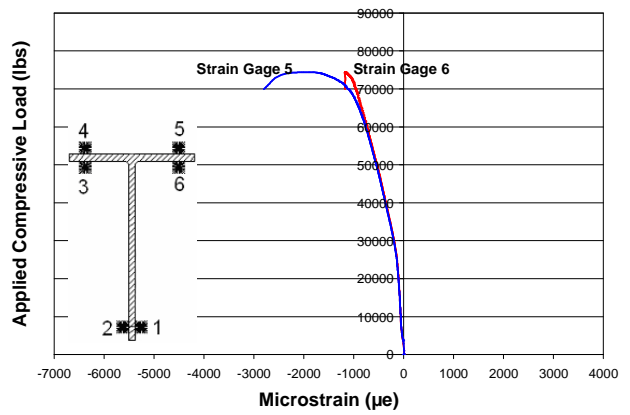
(d) Load-Strain curves.

Figure 4.3 Representative behavior of Control Specimen 90.
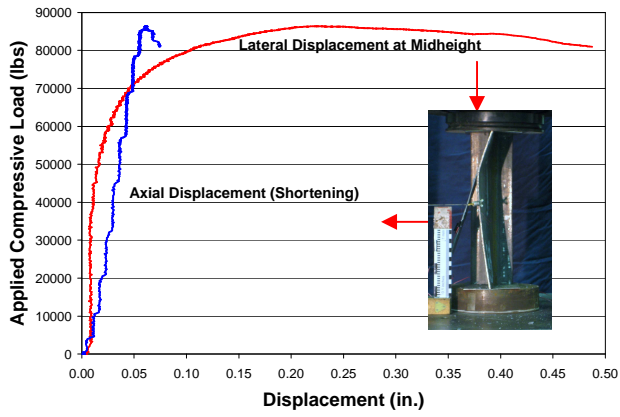
(a) Load-Displacement curves.
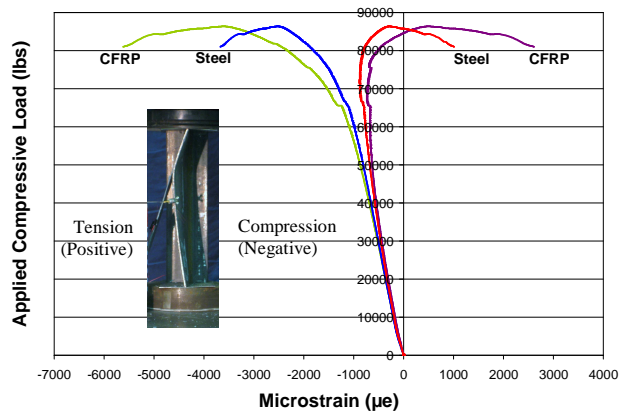
(b) Load-Strain curves.
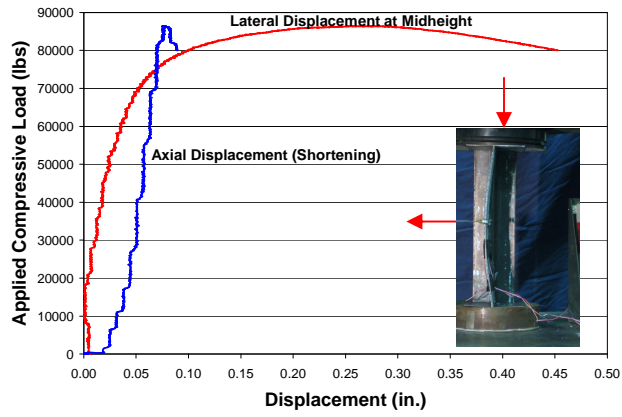
Figure 4.4 Representative behavior of Specimen CFRP-1-50.
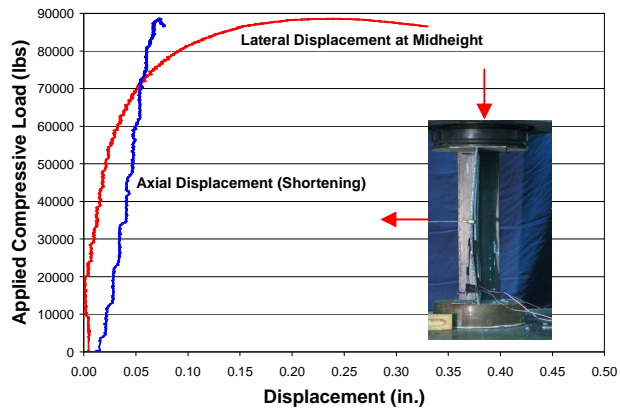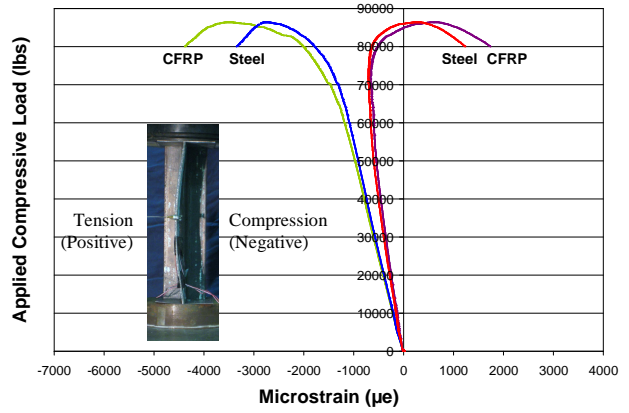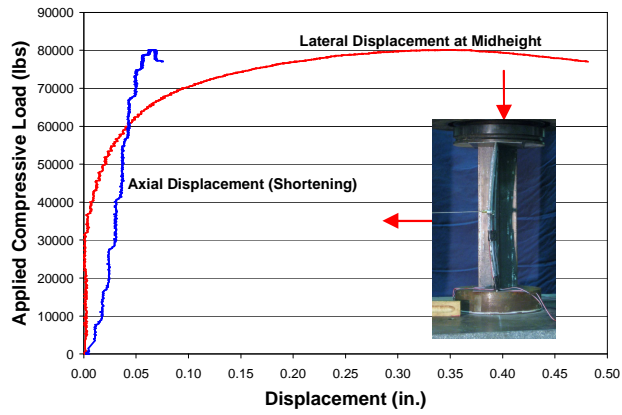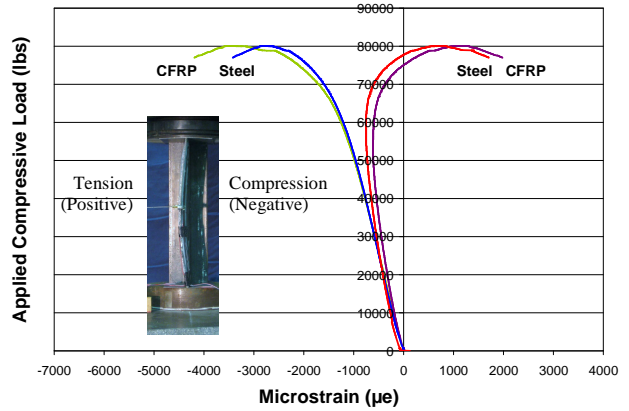

(a) Load-Displacement curves.
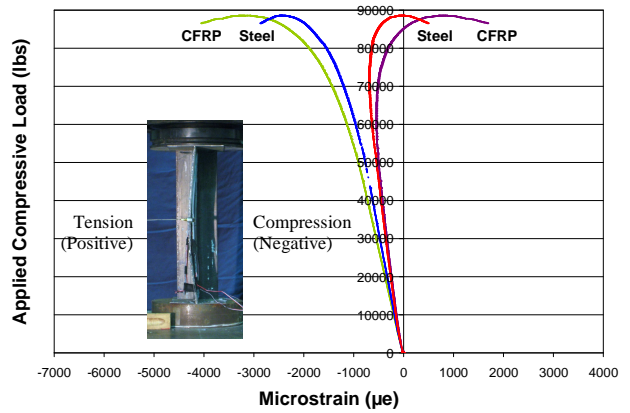
(b) Load-Strain curves.

Figure 4.5 Representative behavior of Specimen CFRP-1-80.
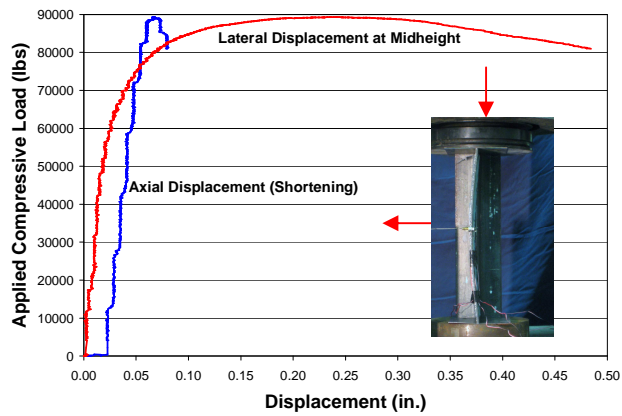
(a) Load-Displacement curves.

(b) Load-Strain curves.

Figure 4.6 Representative behavior of Specimen CFRP-1-90.

(a) Load-Displacement curves.

(b) Load-Strain curves.

Figure 4.7 Representative behavior of Specimen CFRP-2-50.

(a) Load-Displacement curves.

(b) Load-Strain curves.

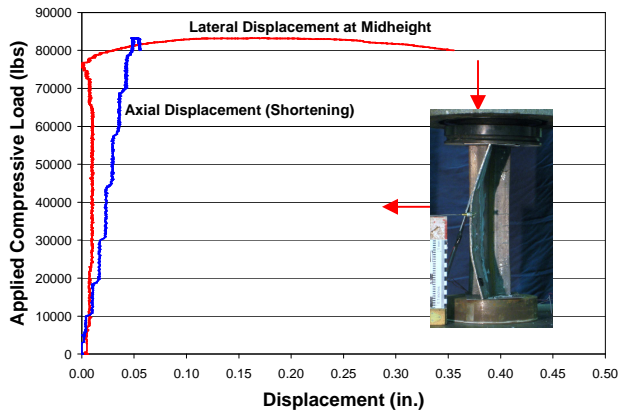**Figure 4.8** Representative behavior of Specimen CFRP-2-80.
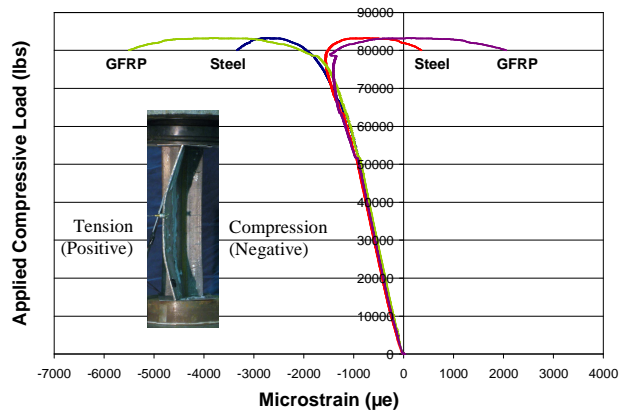

(a) Load-Displacement curves.

(b) Load-Strain curves.

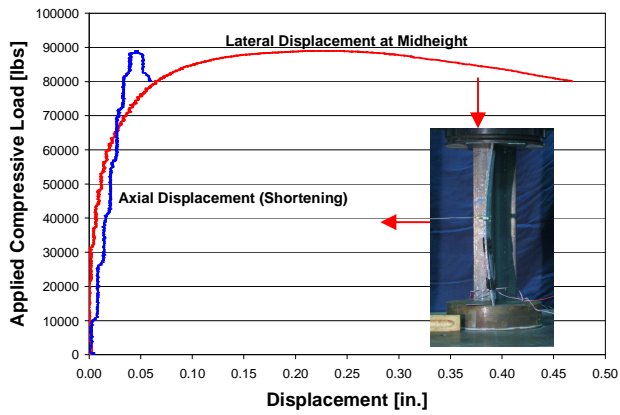**Figure 4.9** Representative behavior of Specimen CFRP-2-90.

(a) Load-Displacement curves.   (b) Load-Strain curves.

Figure 4.10 Representative behavior of Specimen GFRP-1-50.

(a) Load-Displacement curves.   (b) Load-Strain curves.

Figure 4.11 Representative behavior of Specimen GFRP-1-80.
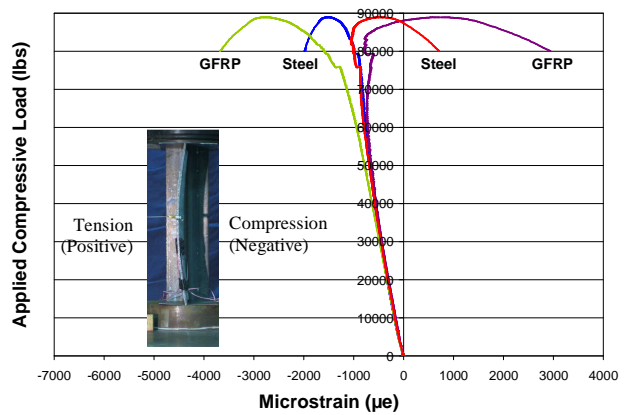
(a) Load-Displacement curves.

(b) Load-Strain curves.

Figure 4.12 Representative behavior of Specimen GFRP-1-90.

(a) Load-Displacement curves.

(b) Load-Strain curves.

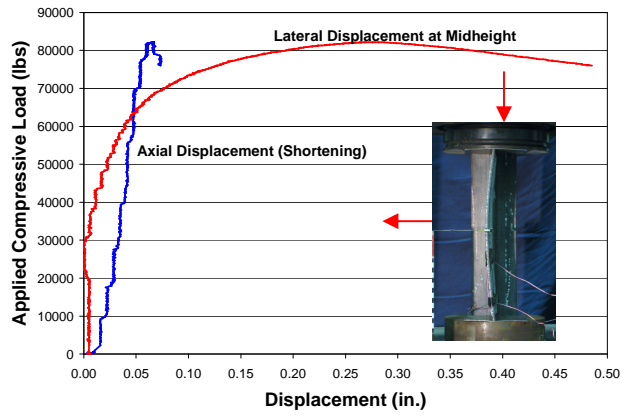**Figure 4.13** Representative behavior of Specimen GFRP-2-50.
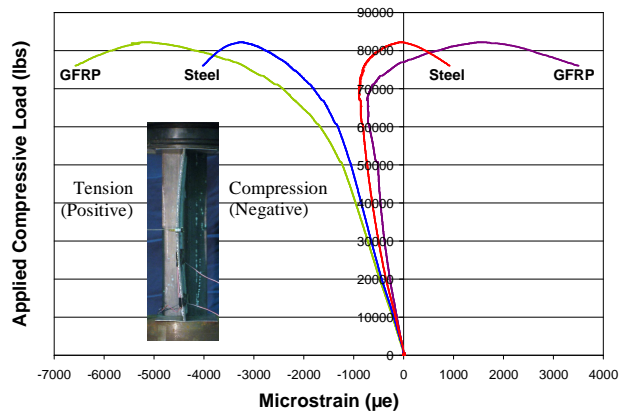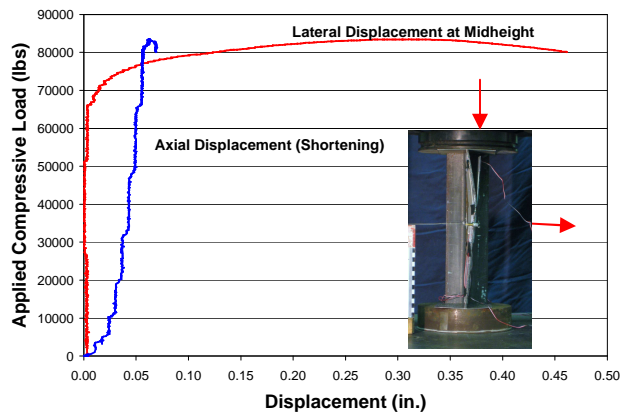
(a) Load-Displacement curves.
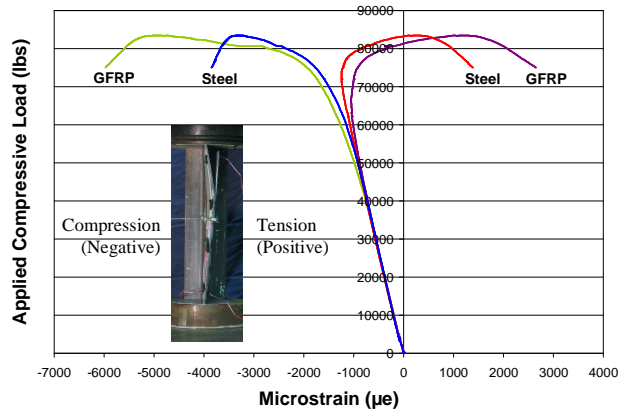
(b) Load-Strain curves.
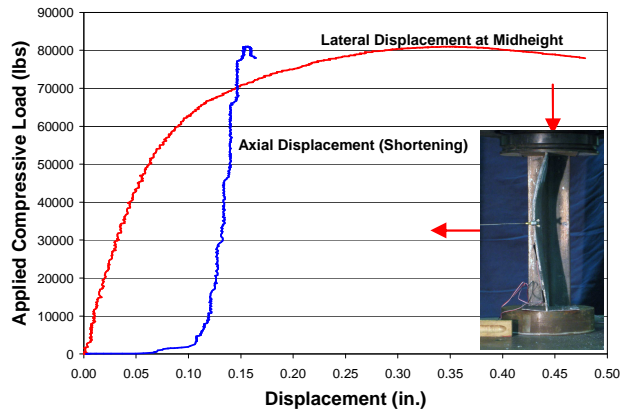
Figure 4.14 Representative behavior of Specimen GFRP-2-80.
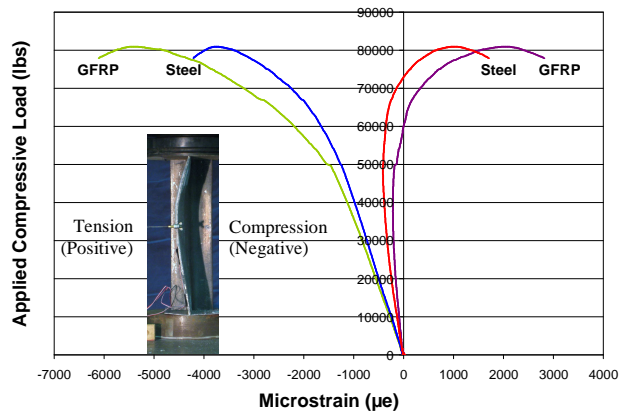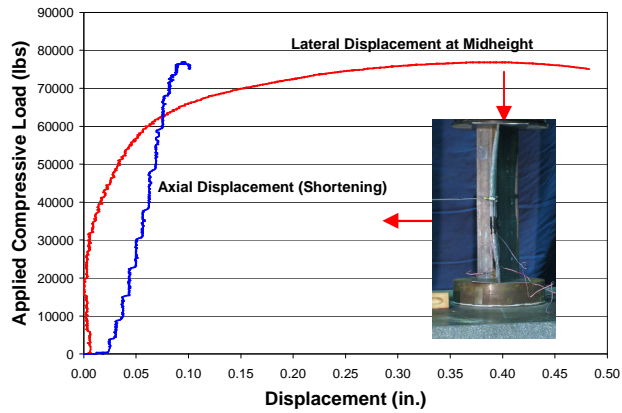

(a) Load-Displacement curves.
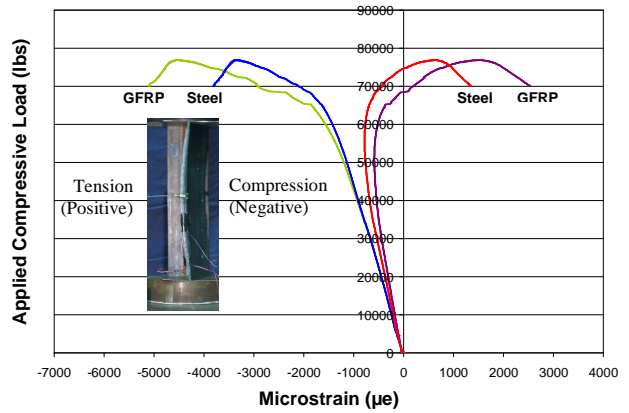
(b) Load-Strain curves.

Figure 4.15 Representative behavior of Specimen GFRP-2-90.

(a)   (b)   (c)
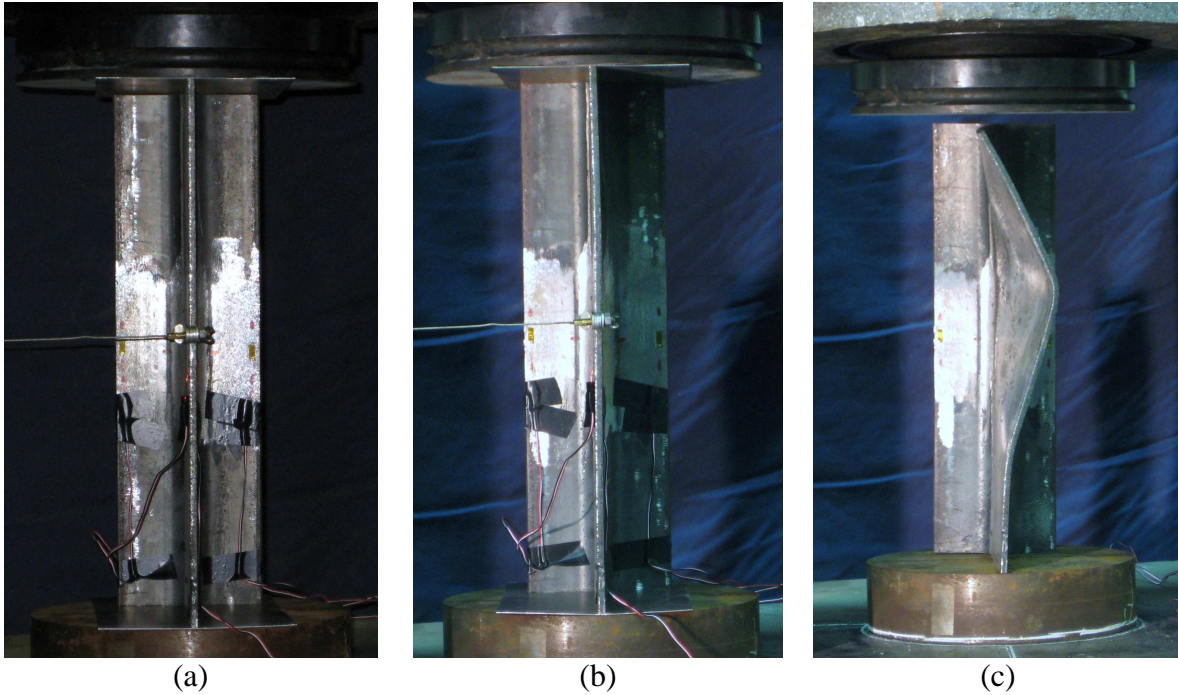
Figure 4.16 Control 50 Specimen.
(a) Prior to loading, (b) at the peak axial load of 80341 lbs (357 kN), and (c) at 50% of axial load capacity.

(a)   (b)   (c)   (d)
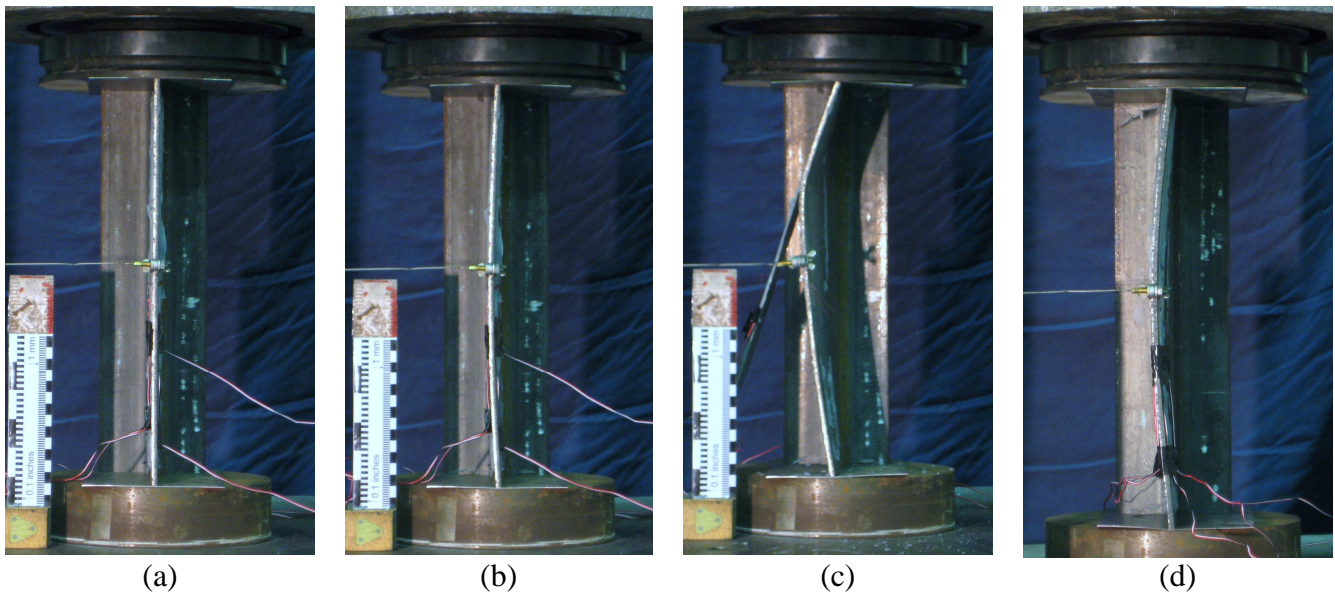
Figure 4.17 Specimens CFRP-1-50 and CFRP-1-90.
(a) CFRP-1-50 prior to loading, (b) CFRP-1-50 at the peak axial load of 86419 lbs (384 kN), (c) CFRP-1-50 at 50% of axial load capacity, (d) CFRP-1-90 at 90% axial load capacity.
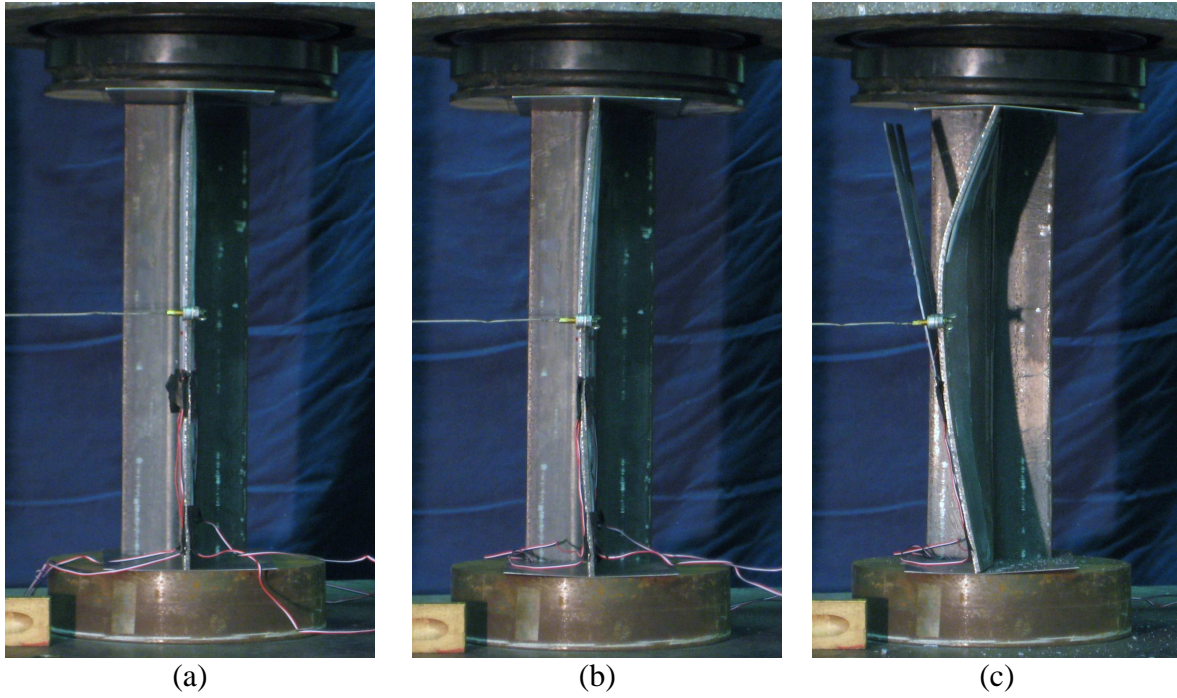
Figure 4.18 Specimen CFRP-2-50.
(a) Prior to loading, (b) at the peak axial load of 82742 lbs (368 kN), and (c) at 50% of axial load capacity.
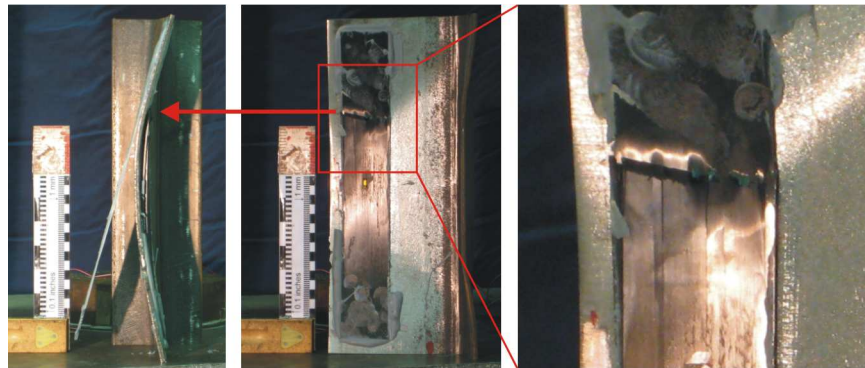
Figure 4.19 Specimen CFRP-2-90 showing compressive failure of bonded CFRP.

| (a) | (b) | (c) |
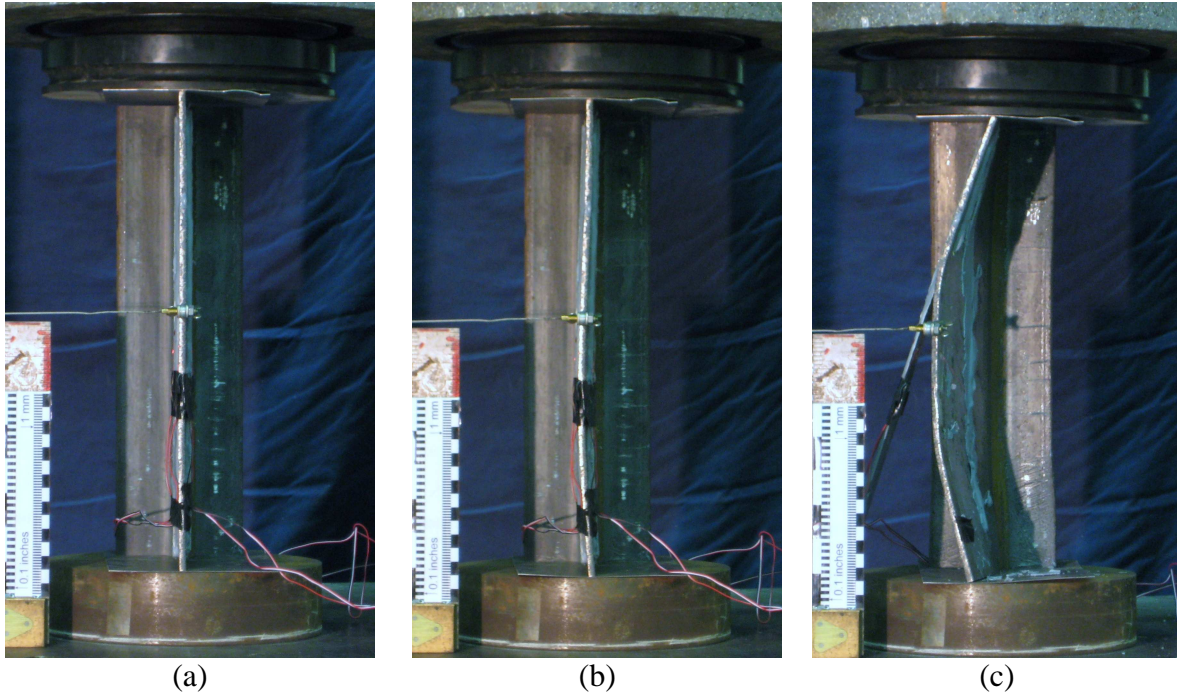
Figure 4.20 Specimen GFRP-1-50.
(a) Prior to loading, (b) at the peak axial load of 83247 lbs (370 kN), and (c) at 50% of axial
load capacity.

| (a) | (b) | (c) |
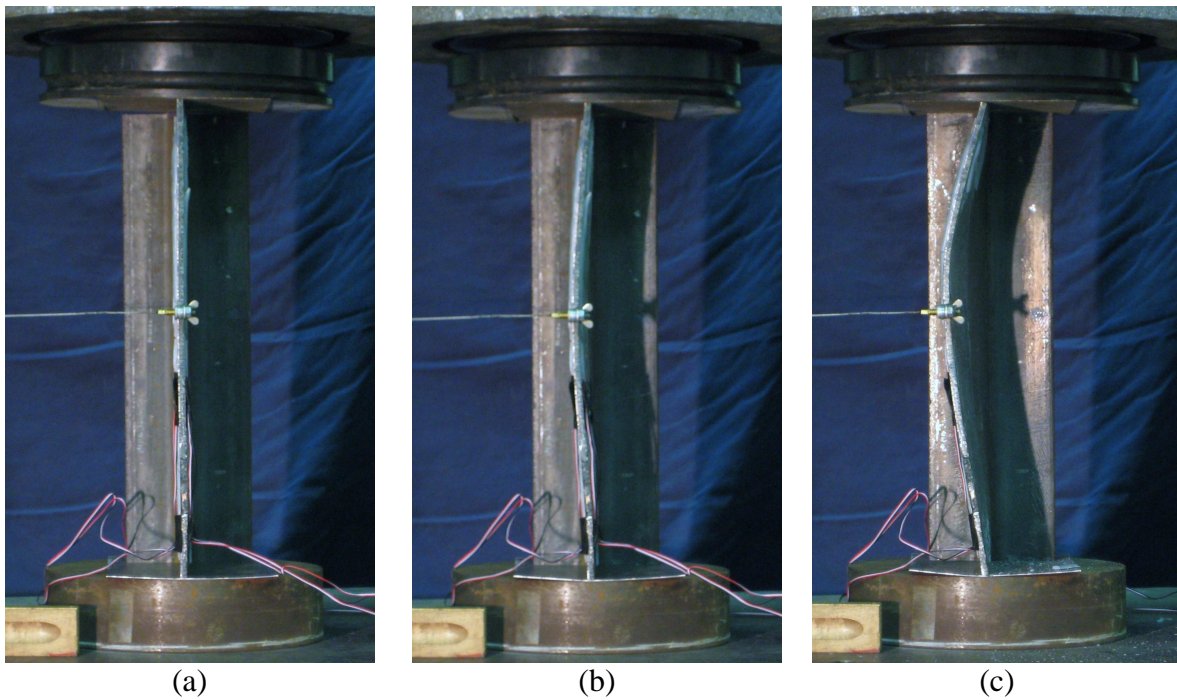
Figure 4.21 Specimen GFRP-2-50.
(a) Prior to loading, (b) at the peak axial load of 80966 lbs (360 kN), and (c) at 50% of axial
load capacity.
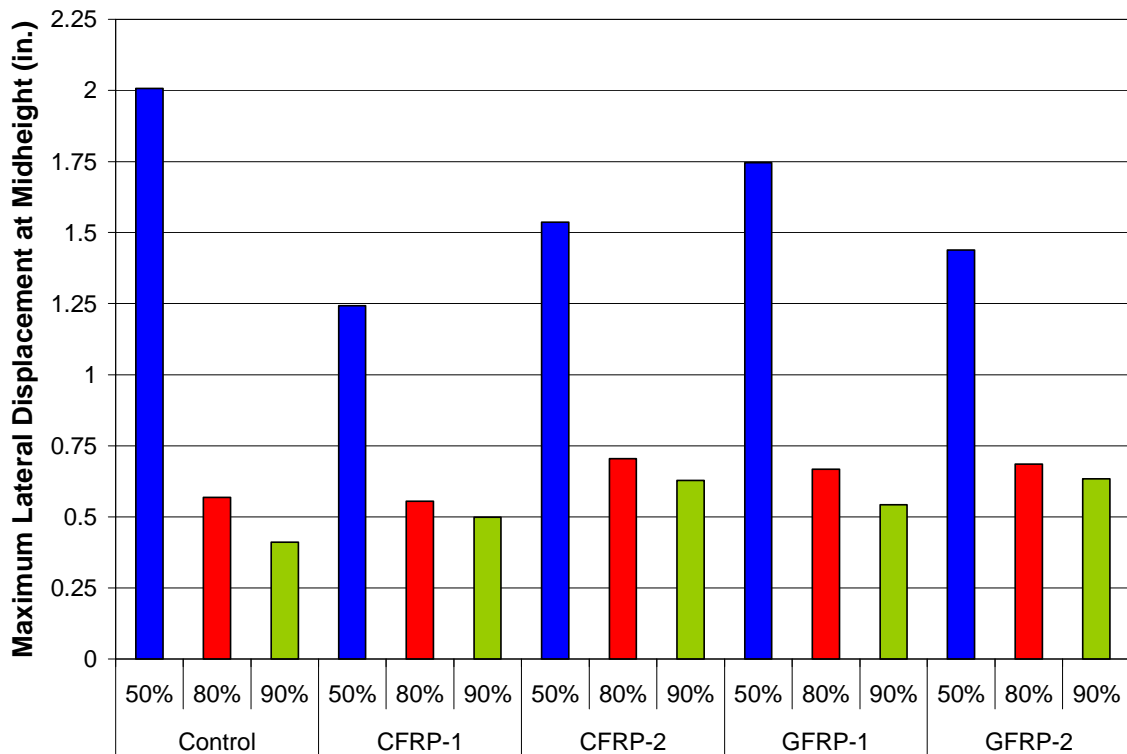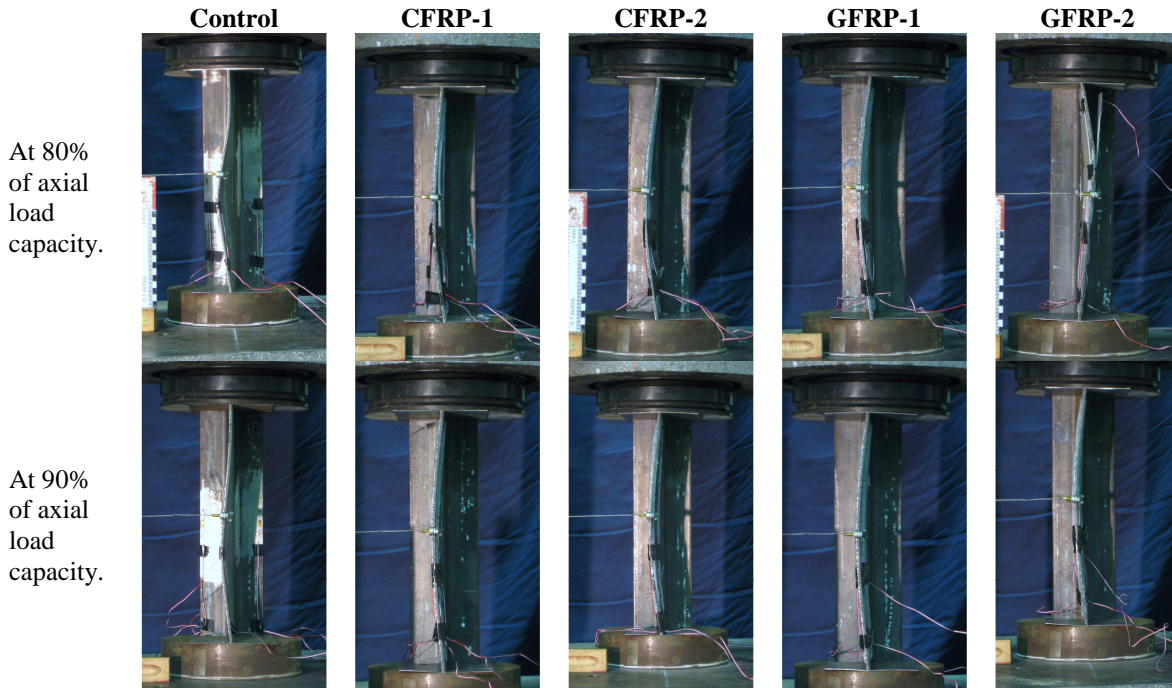
Figure 4.22 Maximum lateral displacements at midheight including representative photographs of the specimens at both 80% and 90% of the axial load capacity.

5.0   EXPERIMENTAL DISCUSSION

This chapter deals with the interpretation and discussion of the data and results presented in Chapter 4. A summary of the peak load behavior is provided in Table 5.1. It is seen that the presence of the FRP results in a marginal improvement in axial load carrying capacity. This effect, as expected, is shown to be proportional to the increase in radius of gyration affected by the presence of the GFRP.

5.1   WEB BIFURCATION LOAD

The web local buckling bifurcation load is the applied load at which web local buckling at the tip of the stem is initiated. Prior to bifurcation, the strain gages on either side of the web (gages 1 and 2) essentially "track" each other in compression indicating the web stem is subject to uniform compression (as shown in Figure 4.4, for example). As buckling initiates, the web bends resulting in a superimposed strain gradient through the thickness of the web. This behavior is easily represented as the application of a moment to the web equal to the applied axial load multiplied by an apparent eccentricity of this load; that is: P x e as shown in Figure 5.1. Once this eccentricity is introduced, one gage continues to increase in compression at a greater rate than the application of axial load would suggest and the second gage begins shedding compression, eventually going into

net tension. The bifurcation load is arbitrarily defined in this work as occurring when the axial resultant acting on the web stem is beyond the dimension of the web; that is the eccentricity of the resultant axial load exceeds half the web width: $e > t_w/2$. The eccentricity is calculated based on the values of strain recorded on gages 1 and 2 (ε_1 and ε_2) as follows (see Figure 5.1):

$$e = \left(\frac{\varepsilon_2 - \varepsilon_1}{\varepsilon_1 + \varepsilon_2} \right) \frac{t_w}{6} \qquad\qquad 5.1$$

The bifurcation loads are reported in Table 5.1. In this test program, bifurcation was seen to initiate above 90% of the peak load attained indicating a very uniform and concentric application of axial load. The presence of the FRP appears to affect the bifurcation load to essentially the same degree as it affects the peak load. The CFRP-1 and GFRP-1 exhibit a marginal increase in the load at which bifurcation initiates reflecting the greater local increase in radius of gyration affected by the FRP discussed in the following section.

5.2   RADIUS OF GYRATION

The slenderness ratio of a member is affected by both the length of the element and its radius of gyration, r_y. When retrofitting steel sections with FRP the objectives are to both increase the maximum compressive capacity of the member while also increasing the radius of gyration to improve the buckling behavior. The more slender a member, the more the member behavior deteriorates under cyclic loading (Bruneau et al., 1998). Decreasing the slenderness of a member ultimately increases the cyclic loading lifespan

as well as its loading capacity. In this experimental program, the WT 6x7 member has a slender stem and a compact flange (see Section 3.7); the retrofit is therefore focused on the stem. Table 5.2 displays the increases in the radii of gyration for the entire WT 6x7 section and for the stem alone (calculated based on the length from the flange to the stem tip, $d - t_f$) when retrofitted with FRP.

The effect of retrofitting is a significant increase in the value of r_y for the stem alone, ranging from 1.12 to 1.36 times the value of r_y for the unretrofit stem (calculated to be 0.058 in.). These increases are proportional to, although approximately three times, the observed increases in axial load carrying capacity and bifurcation load. In contrast, when considering the WT section as a whole, there is essentially no increase of the radius of gyration.

While the axial load capacity was improved by the FRP retrofitting, the increased stem radius of gyration greatly aided in delaying the "kinking" of the stem under axial compression. This results in a more ductile behavior and will ultimately lead to the increased capacity of a member under reversed cyclic axial loading conditions.

5.3   EFFECTS UPON THE STEM IN AXIAL COMPRESSION

Visual observation of the test specimens during and after testing, revealed the improved resistance of the WT stem to "kinking" when FRP is applied (Figure 5.2). In each fiber reinforced specimen, kinking of the stem only occurred after debonding of the FRP. The FRP material inhibited the stem from kinking and ultimately may allow the

70

section to withstand a greater amount of cyclic loading. As discussed above, the increased radius of gyration improved the stability of the stem resulting in a more ductile stem behavior than observed in the control specimens. The stem was supported by the FRP until the eventual debonding of the FRP. The theoretical effect of mitigating the "kinking" effect is illustrated in Figure 5.3. By mitigating kinking:

1. the compression "plateau" *A-B* is elongated;

2. the residual compressive load C_r' may be increased;

3. the "negative stiffness" region (*B-C*) is minimized or mitigated altogether.

4. the reloading tensile stiffness is increased (*C-D-E*); and,

5. the rapid transition in stiffness during tension reloading is less significant, reducing the possibility of an "impact" effect (CISC 2007).

6. the number of cycles to eventual fracture of the section due to low cycle fatigue is increased due to the reduced plastic deformation demand.

Each of these effects results in an increase in energy that may be dissipated by the brace as illustrated by a greater area contained under the hysteresis in Figure 5.3.

71

Table 5.1 Results of plastic buckling tests (Average of three tests in every case).
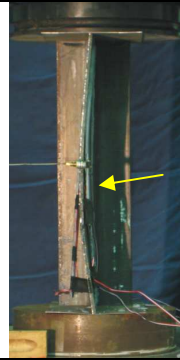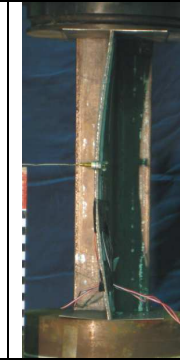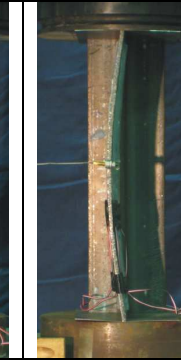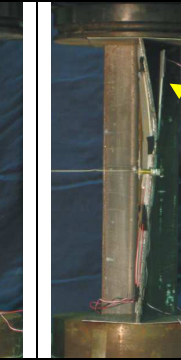
	Control	CFRP-1	CFRP-2	GFRP-1	GFRP-2
Peak axial compression, lbs (kN)	77560 (345)	88125 (392)	83180 (370)	84750 (377)	80480 (358)
ratio of peak load to control peak load	n.a.	1.14	1.07	1.09	1.04
WLB bifurcation load, lbs (kN)	71940 (320)	84305 (375)	78235 (348)	83405 (371)	73515 (327)
ratio of bifurcation load to control bifurcation load	n.a.	1.17	1.09	1.16	1.02
ratio of bifurcation load to peak load	0.93	0.96	0.94	0.98	0.91
Representative photograph taken during post-peak response at axial load of 80% of peak load (Debonding shown by arrows)					
	C	CFRP-1	CFRP-2	GFRP-1	GFRP-2

Table 5.2 Predicted r_y values.
(adapted from Harries and Abraham, 2006)

		calculation	CFRP-1	CFRP-2	GFRP-1	GFRP-2
FRP	t_{FRP}, in		0.11	0.055	0.15	0.075
	b_{FRP}, in		1	2	1	2
	d, in	$= t_{FRP}/2 + t_{stem}/2$	0.155	0.128	0.175	0.138
	A_{FRP}, in^2	$= 2t_{FRP}b_{FRP}$	0.22	0.22	0.3	0.3
	I_{FRP}, in^4	$= (1/12)b_{FRP}t_{FRP}^3 + nA_{FRP}d^2$	0.00427	0.00282	0.00202	0.0012
	n, modular ratio	$= E_{FRP}/E_{steel}$	0.776	0.776	0.207	0.207
WT6x7 Stem Only	t_{stem}, in	*(AISC, 2005a)*	0.200	0.200	0.200	0.200
	d_{stem}, in	$= d - t_f$	5.735	5.735	5.735	5.735
	A_{stem}, in^2	$= t_{stem}d_{stem}$	1.147	1.147	1.147	1.147
	I_{y-stem}, in^4	$= (1/12)\ d_{stem}t_{stem}^3$	0.00382	0.00382	0.00382	0.00382
	r_{y-stem}, in	$= (I_{y-stem}/A_{stem})^{1/2}$	0.0577	0.0577	0.0577	0.0577
	$A_{stem\ comp}$, in^2	$= A_{stem}$ [(1)]	1.147	1.147	1.147	1.147
	$I_{y-stem\ comp}$, in^4	$= I_{y-stem} + nI_{FRP}$	0.0081	0.0066	0.0058	0.0050
	$r_{y-stem\ comp}$, in	$= (I_{y-stem\ comp}/A_{stem\ comp})^{1/2}$	0.0784	0.0710	0.0695	0.0645
	increase in r_y	**$= r_{y-stem\ comp}/r_{y-stem}$**	*1.358*	*1.230*	*1.204*	*1.117*
Full WT6x7 Section	A_{WT6x7}, in^2	*(AISC, 2005a)*	2.08	2.08	2.08	2.08
	I_y, in^4	*(AISC, 2005a)*	1.18	1.18	1.18	1.18
	r_y, in	*(AISC, 2005a)*	0.753	0.753	0.753	0.753
	A_{comp}, in^2	$= A_{stem}$ [(1)]	2.080	2.080	2.080	2.080
	$I_{y\ comp}$, in^4	$= I_y + nI_{FRP}$	1.1833	1.1822	1.1804	1.1802
	$r_{y\ comp}$, in	$= (I_{comp}/A_{comp})^{1/2}$	0.7543	0.7539	0.7533	0.7533
	increase in r_y	**$= r_{y\ comp}/r_y$**	*1.002*	*1.001*	*1.000*	*1.000*

[(1)] $A_{stem\ comp} = A_{comp} = A_{stem}$ due to the low compressive modulus of FRP.

$$P = \left(\frac{\varepsilon_1 + \varepsilon_2}{2}\right) E t_w$$

$$M = \sigma_{bending} S$$

$$\sigma_{bending} = \left(\frac{\varepsilon_2 - \varepsilon_1}{2}\right) E$$

$$S = \frac{t_w^{\,2}}{6}$$

$$e = \frac{M}{P} = \frac{\left(\dfrac{\varepsilon_2 - \varepsilon_1}{2}\right) E \dfrac{t_w^{\,2}}{6}}{\left(\dfrac{\varepsilon_1 + \varepsilon_2}{2}\right) E t_w}$$

$$e = \left(\frac{\varepsilon_2 - \varepsilon_1}{\varepsilon_1 + \varepsilon_2}\right) \frac{t_w}{6}$$
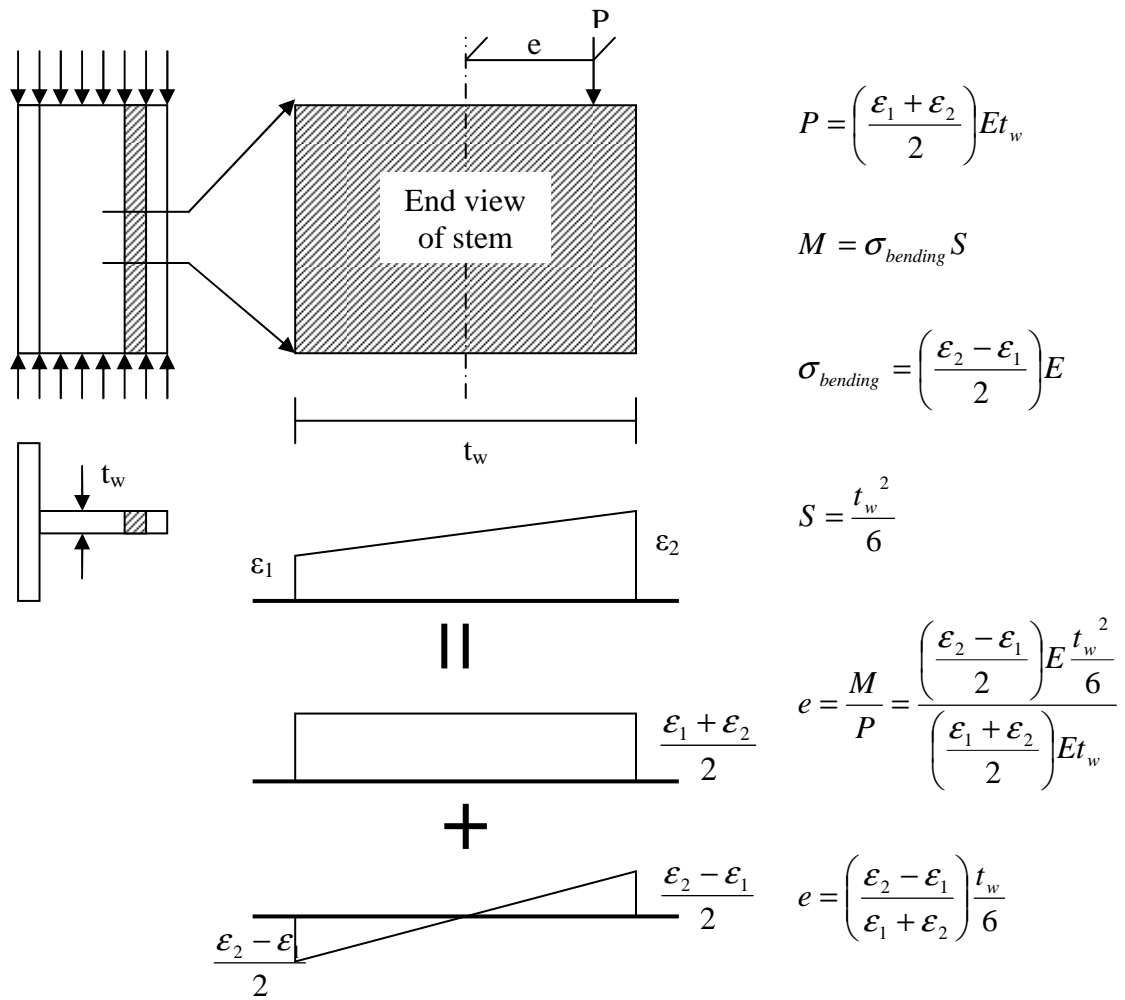
Figure 5.1 Web bifurcation load eccentricity value calculations.

	Pretest	Peak Load	Peak Load	Peak Load	90% of Load Capacity	80% of Load Capacity	50% of Load Capacity
Control							
	(a)	(b)	(c)	(d)	(e)	(f)	(g)
FRP							
	(h)	(i)	(j)	(k)	(l)	(m)	(n)

(a) Pretest of control specimen 50, (b) control specimen 50 peak load of 74400 lbs, (c) control specimen 80 peak load of 77800 lbs, (d) control specimen 90 peak load of 80400 lbs, (e) at 90% of post peak axial load capacity, (f) at 80% of post peak axial load capacity, (g) at 50% of post peak axial load capacity, (h) pretest of GFRP-1-50, (i) GFRP-1-50 peak load of 84100 lbs, (j) CFRP-1-80 peak load of 89800 lbs, (k) CFRP-1-90 peak load of 90400 lbs, (l) CFRP-1-90 at 90 % of post peak axial load capacity, (m) CFRP-1-80 at 80 % of post peak axial load capacity, and (n) GFRP-1-50 at 50 % of post peak axial load capacity.

Figure 5.2 Photographic representations of the effects of fiber reinforcement on the behavior of the stem under axial compression.
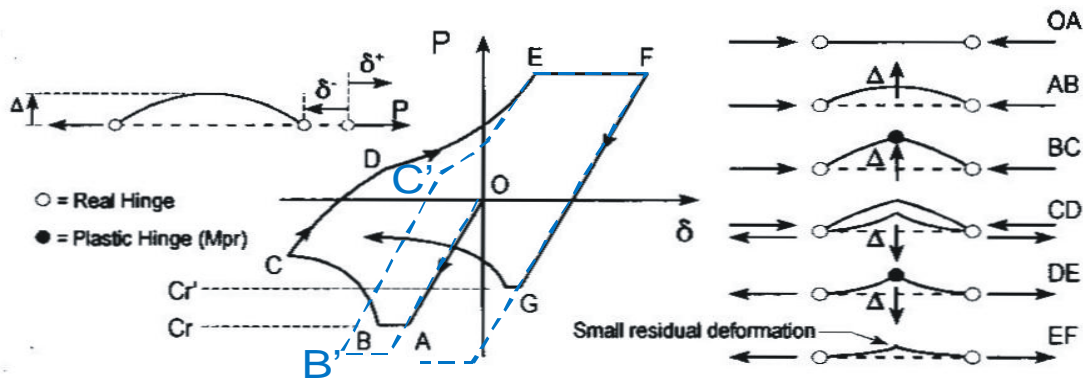
Figure 5.3 Modified sample hysteresis of brace under cyclic loading to illustrate the effect of the absence of kink formation. (original from Bruneau, 1998, adapted from Harries and Abraham, 2006)

6.0   CONCLUSIONS AND RECOMMENDATIONS

This section presents the conclusions of the experimental program, and recommendations based on these conclusions.

6.1   CONCLUSIONS

The concept of strategically applying FRP material to a steel compression member in order improve local buckling behavior was proposed and investigated in this pilot study. The nominal affect of the addition of small amounts of FRP has little effect on the elastic buckling behavior of the long sections typical of braces found in building structures (Abraham, 2006). The FRP retrofit is however able to affect local behavior. Improvement in load-carrying capacity is proportional to the increase in effective radius of gyration (r_y) affected by the presence of the FRP. For elastic buckling, the entire section is considered in which case the increase in r_y is nominal. For plastic buckling, only the outstanding plate element (WT stem, in the present case) is considered in which case the proportional improvement in capacity is greater.

Prior to FRP debonding, the presence of the FRP controls the plastic buckling and delays the formation of the plastic "kink". The formation of this kink affects the cyclic compressive capacity of the section upon subsequent reloading, the tensile stiffness of the

section, and can lead to section fracture in relatively few loading cycles. Thus the application of FRP may represent a viable option for improving the energy absorption and ultimate cyclic ductility of elements susceptible to plastic buckling in a seismic lateral force resisting system. The following conclusions were arrived at through this experimental program:

1. The FRP retrofit measures did not provide a substantial increase in the axial compression load carrying capacity of the WT steel section members. The CFRP-1 and CFRP-2 specimens exhibited an increase in axial capacity of 14% and 7%, respectively. The GFRP-1 and GFRP-2 specimens exhibited an increase in axial capacity of 9% and 4%, respectively.

2. In this test program, bifurcation was seen to initiate above 90% of the peak axial load attained indicating a very uniform and concentric application of axial load. The presence of the FRP appears to affect the bifurcation load to essentially the same degree as it affects the peak load. The CFRP-1 and GFRP-1 specimens exhibited a marginal increase in the load at which bifurcation initiated reflecting the greater local increase in radius of gyration affected by the FRP.

3. The effect of retrofitting is a significant increase in the value of r_y for the WT stem alone, ranging from 1.12 to 1.36 times the value of r_y for the unretrofit stem. These increases are proportional to, although approximately three times, the observed increases in axial load carrying capacity and bifurcation load. In contrast, when considering the WT section as a whole, there is essentially no increase of the radius of gyration.

4. While the axial load carrying capacity was improved by the FRP retrofitting, the FRP was most effective in delaying the "kinking" of the stem under axial compression. This results in a more ductile behavior and will ultimately lead to increased capacity of a member under reversed cyclic axial loading conditions.

5. Visual observation of the test specimens during and after testing, revealed the improved resistance of the WT stem to "kinking" when FRP is applied (Figure 5.2). In each FRP specimen, kinking of the stem only occurred after debonding of the FRP. The FRP material inhibited the stem from kinking and ultimately may allow the section to withstand a greater amount of cyclic loading. The stem was supported by the FRP until the eventual debonding of the FRP. The FRP, in this case, may serve to "spread" the plastic behavior over a larger region of the WT stem.

6. The effectiveness of the FRP is limited by its ability to remain affixed to the steel substrate under axial compression load. The debonding behavior may be described as "end-peel" debonding. The end peel behavior of the FRP from the steel substrate is linked to the strains due to curvature and the interfacial shear caused by this curvature at the termination of the bonded FRP.

6.2   RECOMMENDATIONS

Recommendations for future study include:

1. The application of FRP composite retrofitting should be explored in areas of moderate and high seismic activity. The large impact that the FRP had on delaying "kinking" behavior of the WT stem suggests the need to explore this behavior under reversed cyclic axial loading conditions.

2. Investigating the effects of the FRP development lengths on steel members to which the FRP composite materials are applied. This in turn may lead to further investigation of the impact of bond adhesion to the steel substrate, and ways in which to improve the bond behavior. The improvement of bonding FRP composite materials to the steel substrate will enhance the effectiveness of the FRP.

3. Related to the previous recommendation, methods of providing FRP anchorage where extension of the FRP is not an option (such as in flexural hinges in beams at column faces) should be investigated to maximize the usability of the concept of FRP stabilization.

The field of FRP composite materials is relatively new, leaving much more investigation on the effects of FRP on steel members still left to be done. The vast array of practical applications of FRP in the field of civil engineering has only yet to be discovered.

APPENDIX

APPARENT CENTROID LOCATION

Actual Centroid Calculation

Load at which the stresses and strains were calculated: 10,049 lbs

Strains [μe]:

$\varepsilon_{W1} := 296$ $\varepsilon_{F1} := 244$ $\varepsilon_{F3} := 345$

$\varepsilon_{W2} := 239$ $\varepsilon_{F2} := 245$ $\varepsilon_{F4} := 337$

T Cross-Sectional Properties

$t_f := 0.225$ $E_s := 29000$

$t_w := 0.2$

$b_f := 1.985$

$b_w := 5.736$

$b_{gage} := 0.25$

Stresses [ksi]:

$\sigma_{W1} := \dfrac{29000 \cdot \varepsilon_{W1}}{10^6}$ $\sigma_{W1} = 8.584$

$\sigma_{W2} := \dfrac{29000 \cdot \varepsilon_{W2}}{10^6}$ $\sigma_{W2} = 6.931$

$\sigma_{F1} := \dfrac{29000 \cdot \varepsilon_{F1}}{10^6}$ $\sigma_{F1} = 7.076$

$\sigma_{F2} := \dfrac{29000 \cdot \varepsilon_{F2}}{10^6}$ $\sigma_{F2} = 7.105$

$\sigma_{F3} := \dfrac{29000 \cdot \varepsilon_{F3}}{10^6}$ $\sigma_{F3} = 10.005$

$\sigma_{F4} := \dfrac{29000 \cdot \varepsilon_{F4}}{10^6}$ $\sigma_{F4} = 9.773$

Average the stress between the pairs of strain gages:

$A_1 := \dfrac{\sigma_{F3} + \sigma_{F4}}{2}$ $A_1 = 9.889$

$A_2 := \dfrac{\sigma_{F1} + \sigma_{F2}}{2}$ $A_2 = 7.091$

$A_3 := \dfrac{\sigma_{F1} + \sigma_{F3}}{2}$ $A_3 = 8.54$

$A_4 := \dfrac{\sigma_{W1} + \sigma_{W2}}{2}$ $A_4 = 7.758$

Stress Distribution Found Through Linear Interpretation

$Avg1 := -3.47 \cdot \dfrac{A_2 - A_1}{2.97} + A_2$ $Avg1 = 10.36$

$Avg2 := 3.47 \cdot \dfrac{A_2 - A_1}{2.97} + A_1$ $Avg2 = 6.619$

$Avg3 := A_3$ $Avg3 = 8.54$

$Avg4 := 5.735 \cdot \dfrac{A_4 - A_3}{5.235} + A_3$ $Avg4 = 7.683$

Locations upon which the force acts:

$d_{1x} := 0.1125$ $d_{1y} := 0$ $d_{4x} := 0.1125$ $d_{4y} := 3.397$

$d_{2x} := 0.1125$ $d_{2y} := .2$ $d_{5x} := 4$ $d_{5y} := 1.985$

$d_{3x} := 0.1125$ $d_{3y} := 3.197$ $d_{6x} := 4.2$ $d_{6y} := 1.985$

Flange Calculations

$h_1 := \text{if}(\text{Avg1} < \text{Avg2}, \text{Avg1}, \text{Avg2})$ $h_3 := \text{if}\left[\text{Avg1} < \text{Avg2}, \left(\dfrac{\text{Avg2} - \text{Avg1}}{2} + \text{Avg1}\right), \left(\dfrac{\text{Avg1} - \text{Avg2}}{2} + \text{Avg2}\right)\right]$

$h_1 = 6.619$

$\qquad h_3 = 8.49$

$\qquad f_1 := h_1 \cdot t_f \cdot b_f \qquad f_1 = 2.956$

$\qquad\qquad f_3 := h_3 \cdot t_f \cdot b_f$

$h_2 := \text{if}[\text{Avg1} < \text{Avg2}, (\text{Avg2} - \text{Avg1}), (\text{Avg1} - \text{Avg2})]$

$\qquad\qquad f_3 = 3.792$

$h_2 = 3.741$

$\qquad h_4 := \text{if}(\text{Avg1} < \text{Avg2}, \text{Avg2}, \text{Avg1})$

$\qquad f_2 := \dfrac{\dfrac{h_2}{2}}{2} \cdot t_f \cdot b_f$ $h_4 = 10.36$

$\qquad\qquad\qquad f_4 := \dfrac{h_4 - h_3}{2} \cdot t_f \cdot b_f$

$\qquad f_2 = 0.418$

$\qquad\qquad\qquad f_4 = 0.418$

Web Calculations

$h_5 := \text{if}(\text{Avg3} < \text{Avg4}, \text{Avg3}, \text{Avg4})$ $h_6 := \text{if}[\text{Avg3} < \text{Avg4}, (\text{Avg4} - \text{Avg3}), (\text{Avg3} - \text{Avg4})]$

$h_5 = 7.683$ $h_6 = 0.858$

$\qquad f_5 := h_5 \cdot t_w \cdot b_w$ $\qquad f_6 := \dfrac{h_6}{2} \cdot t_w \cdot b_w$

$\qquad f_5 = 8.814$ $\qquad f_6 = 0.492$

$\text{Forces\_Summed} := f_1 + f_2 + f_3 + f_4 + f_5 + f_6$ $\text{Forces\_Summed} = 16.889$

Calculation of New Centroid

$x := \dfrac{f_1 \cdot d_{1x} + f_2 \cdot d_{2x} + f_3 \cdot d_{3x} + f_4 \cdot d_{4x} + f_5 \cdot d_{5x} + f_6 \cdot d_{6x}}{\text{Forces\_Summed}}$ $x = 2.26$

$y := \dfrac{f_1 \cdot d_{1y} + f_2 \cdot d_{2y} + f_3 \cdot d_{3y} + f_4 \cdot d_{4y} + f_5 \cdot d_{5y} + f_6 \cdot d_{6y}}{\text{Forces\_Summed}}$ $y = 1.9$

New Centroid: $x = 2.26$ inches , $y = 1.9$

BIBLIOGRAPHY

Abraham, E.J. (2006). "Conceptual Investigation of Partially Buckling Restrained Braces." MSc Thesis, Department of Civil and Environmental Engineering, University of Pittsburgh, Pittsburgh, PA.

Abraham, E.J. and Harries, K.A. (2007). "Development of "Partial Buckling-Restrained Braces" using FRP", *Proceedings of the ASCE STRUCTURES 07 Congress*, Long Beach CA, May 2007.

Accord, N.B., Earls, C.J., and Harries, K.A., (2006). "On the use of Fiber Reinforced Composites to Improve Structural Ductility in Steel Flexural Members" *Proceedings of the 2006 SSRC-AISC Joint AISC-NASCC Conference*, San Antonio, February 2006.

American Concrete Institute (ACI) Committee 440, (2007) *Report on Fiber-Reinforced Polymer Reinforcement for Concrete Structures*, ACI, Farmington Hills MI, 100 pp. American Institute of Steel Construction (AISC) 2005. *Steel Construction Manual, 13th Edition*.

American Institute of Steel Construction (AISC). (2005a). *Steel Construction Manual, 13th Edition.*

Bruneau, M., Uang, C. M., and A. Whittaker. (1998). *Ductile Design of Steel Structures*, The McGraw-Hill Companies, Boston, Massachusetts, ISBN 0-07-008580-3.

Cadei, J.M.C., Stratford, T.J., Hollaway, L.C. and Duckett, W.G. (2004). "Strengthening Metallic Structures Using Externally Bonded Fibre-Reinforced Polymers," *CIRIA Publication No. C595*. CIRIA, London, 233 pp.

Canadian Institute of Steel Construction CISC). (2007). *Handbook of Steel Construction, 9th Edition*.

Chacon, A., Chajes, M., Swinehart, M., Richardson, D., and G. Wenczel. (2004). "Applications of Advanced Composites to Steel Bridges: A Case Study on the Ashland Bridge." *Proceedings of the 4th Advanced Composites for Bridges and Structures Conference*, Calgary, July 2004.

Ekiz, E. (2007). "Improving Steel Behavior Using Carbon Fiber Reinforced Polymer (CFRP) Wrapping." PhD Thesis, Department of Civil and Environmental Engineering, University of Michigan, Ann Arbor, MI.

Ekiz, E., El-Tawil, S., Parra-Montesinos, G., and S. Goel. (2004). "Enhancing Plastic Hinge Behavior in Steel Flexural Members Using CFRP Wraps." *Proceedings of the 13th World Conference on Earthquake Engineering*, Vancouver, August 2004.

Gillespie Jr., J.W., Mertz, D.R., Kasai, K., Edberg, W.M., Demitz, J.R., and I. Hodgson. (1996). "Rehabilitation of Steel Bridge Girders: Large Scale Testing." *Proceedings of the American Society for Composites 11th Technical Conference*, Atlanta, GA, October 1996.

Harries, K.A., and S. El-Tawil. (2006). "Steel-FRP Composite Structural Systems: State of the Art." *Report to the ASCE Committee on Composite Construction Task Group on Steel-FRP Composite Structures*.

Hollaway, L.C., and J. Cadei. (2002). "Progress in the technique of upgrading metallic structures with advanced polymer composites." Prog. Struct. Engng Mater. 2002, 4, 131-148.

Jones, S.C., and S.A. Civjan. (2003). "Application of Fiber Reinforced Polymer Overlays to Extend Steel Fatigue Life." *Journal of Composites for Construction*, 7(4), 331-338.

Miller, T.C., Chajes, M.J., Mertz, D.R., and J.N. Hastings. (2001). "Strengthening of a Steel Bridge Girder Using CFRP Plates." *Journal of Bridge Engineering*, November/December, 514-522.

Moy, S.S.J. (2004a). "Design Guidelines for the Strengthening of Metallic Structures Using Fibre Reinforced Composites." *Proceedings of the 4th International Conference on Advanced Composite Materials in Bridges and Structures*, Calgary, July 2004.

Moy, S.S.J. (2004b). "Three Case Studies of Carbon Fibre Composite Strengthening of Metallic Structures on the London Underground." *Proceedings of the 4th International Conference on Advanced Composite Materials in Bridges and Structures*, Calgary, July 2004.

Nakashima1, M., Kanao, I., and D. Liu. (2002). "Lateral Instability and Lateral Bracing of Steel Beams Subjected to Cyclic Loading." *Journal of Structural Engineering*, October 2002, 1308-1316.

Nakashima, M., Liu, D., and I. Kanao. (2003). "Lateral-Torsional and Local Instability of Steel Beams Subjected to Large Cyclic Loading." *Steel Structures 3*, 179-189.

Nozaka, K., Shield, C.K., and J.F. Hajjar (2005). "Effective bond length of carbon-fiber-reinforced polymer strips bonded to fatigued steel bridge I-girders." *Journal of Bridge Engineering*, ASCE, v. 10, n. 2, March, pp. 195-205.

Okazaki, T., Liu, D., Nakashima, M., and M.D. Engelhardt. (2006). "Stability Requirements for Beams in Seismic Steel Moment Frames." *Journal of Structural Engineering*, September 2006, 1334-1342.

Patnaik, A.K. and C.L. Bauer. (2004). "Strengthening of Steel Beams with Carbon FRP Laminates." *Proceedings of the 4th International Conference on Advanced Composite Materials in Bridges and Structures*, Calgary, July 2004.

Sayed-Ahmed, E.Y. (2004). "Strengthening of Thin-walled Steel I-Section Beams Using CFRP Strips." *Proceedings of the 4th International Conference on Advanced Composite Materials in Bridges and Structures*, Calgary, July 2004.

Schnerch, D., Stanford, K., Sumner, E., and S. Rizkalla. (2005). "Bond Behavior of CFRP Strengthened Steel Bridges and Structures." *Proceedings of the International Symposium on Bond Behavior of FRP in Structures*, pp 443-451.

Sebastian, W., and S. Luke. (2007). "Interface Failure Mechanics of Elastically (Advanced Composite) Reinforced Steel Members." *Journal of Structural Engineering ASCE*, May 2007, 683-694.

Shaat, A., and A. Fam. (2004). "Strengthening of Short HSS Steel Columns Using FRP Sheets." *Proceedings of the 4th International Conference on Advanced Composite Materials in Bridges and Structures*, Calgary, July 2004, paper No. 093.

Uang, C-M., and C-C. Fan. (2001). "Cyclic Stability Criteria For Steel Moment Connections With Reduced Beam Section." *Journal of Structural Engineering*, Vol. 127, No. 9, pp 1021-1027.

Zhao X-L and Zhang L. (2006). "State-of-the-art review on FRP strengthened steel structures." *Engineering Structures*, Volume 29, Issue 8, 1808-1823.

Published Work Stemming from this Thesis

Harries, K.A., **Peck, A.**, and E.J. Abraham. (2008). "Experimental Investigations of FRP-stabilized Steel Compression Members", *Proceedings of the 4rd International Conference on FRP Composites in Civil Engineering (CICE 2008)*, Zurich, July 2008.

Harries, K.A., Abraham, E.J., and **A. Peck**. (2007). "FRP-stabilized Steel Compression Members", *Proceedings of the Asia-Pacific Conference on FRP in Structures (APFIS 2007)*, Hong Kong, December 2007.